Copy 310

RM A51B20

NACA RM A51B20

NACA

RESEARCH MEMORANDUM

MEASUREMENTS OF DOWNWASH AND SIDEWASH BEHIND CRUCIFORM TRIANGULAR WINGS AT MACH NUMBER 1.4

By Benton E. Wetzel and Frank A. Pfyl

Ames Aeronautical Laboratory
Moffett Field, Calif.

NATIONAL ADVISORY COMMITTEE
FOR AERONAUTICS

WASHINGTON

April 4, 1951

NATIONAL ADVISORY COMMITTEE FOR AERONAUTICS

RESEARCH MEMORANDUM

MEASUREMENTS OF DOWNWASH AND SIDEWASH BEHIND CRUCIFORM TRIANGULAR WINGS AT MACH NUMBER 1.4

By Benton E. Wetzel and Frank A. Pfyl

SUMMARY

The results of an experimental investigation of the downwash and sidewash flow angles in a transverse plane behind a cruciform-wing and body combination are presented. The wing-body combination was composed of a cruciform arrangement of two identical triangular wings of aspect ratio 2.31 corresponding to a leading-edge sweep angle of 60°, placed on a body of fineness ratio of 16. The investigation was conducted at a Mach number of 1.40 and at a Reynolds number of 1.25 million based on the mean aerodynamic chord of the wings. Downwash and sidewash measurements were made for angles of bank of 0°, 11-1/4°, 22-1/2°, and 45° and through an angle-of-attack range of ±8°.

INTRODUCTION

The flow field behind planar wings of low aspect ratio has been shown by recent experiments (references 1, 2, 3, and 4) to be of a more complex character than is indicated by linearized wing theory. The inadequacy of linearized theory led to the development of a more satisfactory theoretical treatment by Spreiter and Sacks in reference 5, wherein the mutual interaction of the vortices and the rolling up of the vortex sheet are considered.

The flow behind cruciform wings is expected to be even more complex, since there is mutual interaction between the distorted vortex sheets from the two wings. It has been the purpose of the present experimental investigation, therefore, to provide information about the flow field behind a cruciform-wing and body combination which may be used for estimating design tail loadings for missiles and for guiding further theoretical analysis.

In the present experiments, surveys of the angles of downwash and sidewash were made behind a representative missile configuration consisting of a fineness ratio 16 body fitted with cruciform triangular wings of aspect ratio 2.31. The measurements were made in a transverse plane essentially perpendicular to the body axis 2.42 mean aerodynamic chord lengths behind the wing trailing edge, a position which is a typical location for missile stabilizing surfaces.

NOTATION[1]

$\bar{c}$ mean aerodynamic chord $\left[\dfrac{\int_0^s c^2\,dy}{\int_0^s c\,dy}\right]$, inches

c local wing chord, inches

s semispan of the wing, where s is measured from body center line, inches

V free-stream velocity, feet per second

x,y,z Cartesian coordinates with the origin located on the body axis 2.42 mean aerodynamic chord lengths behind the trailing edges of the wings (the location of the survey plane). The x axis coincides with the body axis, and the z axis lies in the plane in which the angle of attack was varied. The coordinates have been made nondimensional by dividing by the semispan of the wing.

α angle of attack of body axis, degrees

ϵ angle of downwash, measured from free-stream direction, positive when the flow is directed downward, degrees

ϵ' difference between the angle of downwash at angle of attack and the angle of downwash at $\alpha=0$, degrees

σ angle of sidewash, measured from free-stream direction, positive when the flow is directed to right when viewed from rear, degrees

---

[1]Chord and span dimensions are measured parallel and perpendicular to body center line.

σ' difference between the angle of sidewash at angle of attack and the angle of sidewash at $\alpha=0$, degrees

φ angle of bank, degrees

DESCRIPTION OF APPARATUS

Wind Tunnel

The experimental investigation was made in the Ames 6- by 6-foot supersonic wind tunnel, which is a closed-circuit variable-pressure tunnel. Reference 6 presents a complete description of the wind tunnel.

Model and Support System

The cruciform-wing and body combination used in the experiments had the dimensions shown in figure 1. The wings were identical and had a triangular plan form and an aspect ratio of 2.31 corresponding to a leading-edge sweep angle of 60°. The wings were steel plates 1/4 inch thick, corresponding to 2.63-percent-thickness-chord ratio at the wing-body juncture. The leading and trailing edges were beveled symmetrically on the upper and lower surfaces and finished to approximately 0.001-inch radii. The body was composed of a fineness ratio 6 nose section made of aluminum, and two steel cylindrical sections which were joined together at the trailing edges of the wings by a connecting plug. The connecting plug allowed the nose and the forward cylindrical section, to which the wings were attached, to be rotated through various bank angles with respect to the aft cylindrical section, to which the survey apparatus was attached. The body had a fineness ratio of 16, based on the body length between the apex of the nose and the transverse plane in which the measurements were made.

The wing and body combination was mounted on a cantilever support sting, which is shown in figure 2. The angle of attack of the sting could be varied in a vertical plane through a range of ±5°. A 5° bent sting was used to give angles of attack of the body axis of from 0° to 10°.

Survey Apparatus

Downwash and sidewash measurements were made with a survey apparatus consisting of 27 small cones of 30° included angle, each of which had two pressure orifices diametrically opposed, as is shown in figure 1. This survey apparatus could be pitched relative to the body about an axis of rotation at right angles to the test body axis. With

this arrangement, the axes of the survey cones could be inclined at angles within a range of ±10° with respect to the test body axis. The cones were mounted on two large rakes and on one small rake. The large rakes could be located at alternate positions as is shown in figure 1. The orientations of the survey apparatus for downwash and sidewash measurements are shown in figure 2.

In pitching the survey apparatus about its axis of rotation, the positions of the cones relative to the test body axes were changed. The effect of this variation in cone position will be discussed in the section of this report devoted to precision.

TESTS

Range of Tests

The angles of downwash and sidewash were measured for a range of angle of attack of ±8° for the body axis and for angles of bank of 0°, 11-1/4°, 22-1/2°, and 45°. The angle-of-attack range could not be extended beyond ±8° either because of the limitation in the angle through which the survey apparatus could be rotated or because of the reflection from the tunnel wall of shock waves originating on the model. All data presented in this report were obtained at a Mach number of 1.40 and at a Reynolds number of 1.25 million based on the mean aerodynamic chord. The surveys were made in a plane essentially perpendicular to the body axis located 2.42 mean aerodynamic chord lengths behind the trailing edges of the wings (a typical location for missile stabilizing tail surfaces).

Methods

The incremental changes in downwash angle per incremental change in angle of attack were determined by the null-reading technique. In using this method, the survey apparatus was pitched so that the axes of the cones were inclined at a known angle with respect to the body axis. The wing and body combination and the survey apparatus were then pitched as a unit and the angle of attack recorded when zero pressure difference (null) occurred between the two orifices of each cone. Knowing this angle of attack and the angle of the cone axis relative to the body axis, the downwash angle was readily obtained. This procedure was repeated with the survey apparatus set at various angles with respect to the body axis so that the downwash angle was determined at approximately 2° increments in angle of attack.

For the sidewash-angle investigation, the survey apparatus was rotated 90° about the body axis (as is shown in fig. 2) and then yawed through known angles. The null-reading technique was not used in the sidewash measurements but, rather, various yaw angles of the survey apparatus were set and a photographic record of pressure differences was obtained for each 2° increment of angle of attack. Angles of sidewash corresponding to zero pressure difference were then obtained for each angle of attack from plots of pressure difference versus angle of yaw of the survey apparatus. The pressure difference across each cone was kept sufficiently small to prevent shock detachment.

Reduction of Data

Since the survey rake was attached to the model, the survey cones were moved in the air stream as the angle of attack was varied, and any nonuniformity of the air stream could introduce an error in the results. Consequently, corrections to the measured incremental angles of downwash and sidewash were obtained by measuring the apparent variation of the flow angles with angle of attack at each cone location with the wing and body combination removed from the tunnel. The corrections to the downwash measurements were those due to stream irregularities and varied linearly from 0° at zero angle of attack to a maximum of ±0.2° at an angle of attack of ±8°. Because of the method used in the sidewash measurements, the corrections to the angles of sidewash also included cone errors and were consequently of greater magnitude. In general, the corrections varied almost linearly from 0° at zero angle of attack to a maximum of ±1.0° at an angle of attack of ±8°.

In this report the angles of downwash and sidewash ϵ' and σ', respectively, are incremental angles determined as the difference between the measured angles of flow at the given angle of attack and at $\alpha = 0°$. In this manner, effects other than those due to angle of attack have been eliminated.

In order to plot contours of constant angles of downwash and sidewash and velocity vector fields, it was necessary to determine the angles of flow existing throughout the entire survey field. These angles were obtained by interpolation from plots of the measured angles of flow as functions of the distances from the vertical and horizontal planes through the axis of the body. The latter curves were faired in such a manner that the conditions of continuity and irrotation were satisfied everywhere outside the vortex wake for two-dimensional incompressible flow in the transverse plane in which the flow surveys were made. Since measurements were made for only one-half the flow field,

use was made of the data obtained at negative angles of attack to determine the angles of flow in the other half of the field at positive angles of attack.

Precision

The accuracy of the experimental data has been estimated by considering the uncertainties in the following factors:

Angular measurement.- The estimated uncertainty in both the angles of downwash and angles of sidewash was $\pm 0.1^\circ$ due to angular measurement as determined by the square root of the sum of the squares of the uncertainties in the following measurements:

1. The angle of attack of the test body

2. The angle of rotation of the survey apparatus both for tests with the wing and body combination in place and for the stream calibration

A cathetometer was used to measure the angle of attack of the model during the operation of the wind tunnel. The uncertainty of the angle-of-attack measurements with this instrument was $\pm 0.05^\circ$. The angle of rotation of the survey apparatus was measured with a vernier protractor with a least count of 0.1° and could be read to within one-half of the least count.

Displacement of cones.- As was noted in the section of this report devoted to survey apparatus, when the survey apparatus was pitched and yawed about its axis of rotation the cones were displaced relative to the test body axes. The uncertainties resulting from lateral displacements of the cones have been estimated on the basis of the actual displacements and the gradients existing in the flow field. In general, the uncertainties due to these displacements were not greater than $\pm 0.2^\circ$ at an angle of attack of $\pm 8^\circ$ for both angles of downwash and sidewash. At smaller angles of attack the uncertainties were of smaller magnitude. The uncertainties in the downwash and sidewash measurements due to longitudinal movement of the cones relative to the test body are believed to be negligible, since the downwash and sidewash angles vary only to a small degree in the longitudinal direction in regions where the vortex sheet is essentially rolled up into discrete vortices.

In summary on the basis of these uncertainties, the total uncertainty in measuring the angles of downwash and sidewash is estimated to be slightly less than $\pm 0.25^\circ$ at an angle of attack of $\pm 8^\circ$. At smaller angles of attack the uncertainties are of smaller magnitude.

RESULTS AND DISCUSSION

The results of the experimental investigation given as angles of downwash and sidewash are presented for various angles of bank of the cruciform-wing and body combination and angles of attack of the body axis. If the reader desires to convert to angles of yaw and pitch, the transfer equations of reference 7 may be used.

The results have been presented in three forms: (1) tabulated angles of downwash and sidewash at various angles of bank as a function of angle of attack, (2) contours of constant angles of downwash and sidewash, and (3) velocity vector fields.

The tabulated results for an angle-of-attack range of $\pm 8^\circ$ are presented in table I. For the angles of downwash it was necessary to determine the values from curves faired through the experimental values.

In order that the results of this investigation could be applied to an estimation of the loading of various tail designs, contours of constant angles of downwash and sidewash have been plotted for angles of attack of 2°, 4°, 6°, and 8°. Figures 3, 4, 5, and 6 present these contours for bank angles of 0°, $11\text{-}1/4^\circ$, $22\text{-}1/2^\circ$, and 45°, respectively. The contours have been drawn for every 0.5° of induced angularity in the flow field, except in figure 5(d), where the gradient was too great to include all contours. Dashed contours indicate values of downwash and sidewash angles obtained by applying the conditions of continuity and irrotation to the limited measurements which were available in these regions. In general, insufficient measurements were obtained near the body, and it will be observed that some contours have not been closed in this region.

The flow in the survey plane can be visualized more easily through the use of velocity vector fields. Such fields have been presented in figures 7, 8, 9, and 10 for angles of attack of 4° and 8° and for angles of bank of 0°, $11\text{-}1/4^\circ$, $22\text{-}1/2^\circ$, and 45°. The vectors shown represent the magnitude and direction of the transverse flow velocities at the position indicated by the tail end of the vector. These vector fields permit the loading of lifting surfaces to be estimated through the use of the parameter $d\epsilon/d\alpha$ which can be obtained approximately by comparing the length of the downwash component of the velocity vectors with the vector αV shown at the bottom of the figures. Inasmuch as the variation of ϵ with a change in angle of attack α is not linear, an accurate estimate of $d\epsilon/d\alpha$ at a given angle of attack necessitates plotting ϵ as a function of α.

In the subsequent portion of this report these results are discussed only briefly since, in the interests of expediting the release of this information, only a cursory analysis has been made.

(a) $\varphi = 0^\circ$: At an angle of bank of 0°, the vertical wing carries no lift, and the wing-body combination is essentially equivalent for the present problem to a plane-wing and body combination. Velocity vector fields for this angle of bank are shown in figure 7. The theoretical location of the vortex sheet in the transverse plane in which the measurements were made has been indicated by the dashed lines. The vortex sheet was obtained from the results of calculations performed by Westwater in reference 8 for a wing with elliptic span loading, wherein the continuous sheet was replaced by 20 discrete line vortices and the motion of each vortex calculated step by step. Westwater's results were applied to the present problem by relating his time factor to the distance behind the wing as indicated in reference 5. The calculated position of each of the vortices in the transverse plane has been located by a small cross. In general, the directions of the experimental velocity vectors are those which might be expected to result from such distributions of vorticity.

It will be observed that the distortion of the vortex sheet increases with an increase in angle of attack. Since the downwash depends upon the shape of the vortex sheet as well as the lift, it is to be expected that nonlinear pitching-moment characteristics will exist for a stabilizing surface placed in this field.

(b) $\varphi = 11\text{-}1/4^\circ$: As the model is banked, the wing which was vertical at zero angle of bank begins to carry lift when the angle of attack is increased. At an angle of bank of $11\text{-}1/4^\circ$, however, the vortices shed from the tips of this wing are weak and are not discernible in the data. It can be observed in figure 8 that there is no plane of symmetry in the flow field and that, in general, there are large induced velocities throughout the upper half of the flow-field and in the region below the right wing panel. The estimated position of the vortex cores shown by the dashed circles in figure 8 shows the movement of the vortex cores with angle of attack to be nonlinear, a factor which may contribute nonlinear moment characteristics for the stabilizing surfaces placed in such a flow field.

(c) $\varphi = 22\text{-}1/2^\circ$: When the angle of bank is $22\text{-}1/2^\circ$, the velocity vector field (fig. 9) indicates the existence of four vortices in the flow field, one of which is not clearly discernible at an angle of attack of 4°. It can be seen that, at this angle of bank, also, no plane of symmetry exists in the flow. The mutual interaction of the four vortices results in complex variations in the angles of sidewash and downwash throughout the flow field. These data indicate that in

addition to nonlinear pitching-moment characteristics, it is to be expected that significant rolling moments may result from placing the stabilizing surfaces of a missile in this flow field.

(d) $\varphi = 45^\circ$: When the wing-body combination is banked 45°, the flow again has a plane of symmetry, and two pairs of vortices appear as shown in the velocity vector fields of figure 10. These vector fields show large downwash velocities near the plane of symmetry, with larger velocities in the upper half of the flow field. Large sidewash velocities exist in this region and in the region near the tips of the lower wing panels. A comparison of the velocity vector fields for angles of attack of 4° and 8° indicates that, because of the large values of downwash along the horizontal axis at an angle of attack of 8°, an interdigitated tail of small span will be less effective in contributing to the static longitudinal stability of a missile than an in-line tail when the wings are banked 45°.

Ames Aeronautical Laboratory,
National Advisory Committee for Aeronautics,
Moffett Field, Calif.

REFERENCES

1. Perkins, Edward W., and Canning, Thomas N.: Investigation of Downwash and Wake Characteristics at a Mach Number of 1.53. I - Rectangular Wing. NACA RM A8L16, 1949.

2. Perkins, Edward W., and Canning, Thomas N.: Investigation of Downwash and Wake Characteristics at a Mach Number of 1.53. II - Triangular Wing. NACA RM A9D20, 1949.

3. Adamson, D., and Boatright, William B.: Investigation of Downwash, Sidewash, and Mach Number Distribution Behind a Rectangular Wing at a Mach Number of 2.41. NACA RM L50G12, 1950.

4. Walker, Harold J., and Stivers, Louis S., Jr.: Investigation of the Downwash and Wake Behind a Triangular Wing of Aspect Ratio 4 at Subsonic and Supersonic Mach Numbers. NACA RM A50I14a, 1950.

5. Spreiter, John R., and Sacks, Alvin H.: The Rolling up of the Trailing Vortex Sheet and Its Effect on the Downwash Behind Wings. Jour. Aero. Sci., vol. 18, no. 1, Jan. 1951, pp. 21-32.

6. Frick, Charles W., and Olson, Robert N.: Flow Studies in the Asymmetric Adjustable Nozzle of the Ames 6- by 6-Foot Supersonic Wind Tunnel. NACA RM A9E24, 1949.

7. Spreiter, John R.: Aerodynamic Properties of Cruciform-Wing and Body Combinations at Subsonic, Transonic, and Supersonic Speeds. NACA TN 1897, 1949.

8. Westwater, F. L.: Rolling Up of the Surface of Discontinuity Behind an Aerofoil of Finite Span. R. & M. No. 1692, British A.R.C., 1935.

TABLE I.- ANGLES OF DOWNWASH AND SIDEWASH

(a) $\Phi=0^\circ$.

$\frac{z}{s}$	$\frac{y}{s}$	ϵ', degrees								
		$\alpha=-8^\circ$	-6°	-4°	-2°	0°	2°	4°	6°	8°
1.43	0	-0.4	-0.4	-0.4	-0.2	0	0.2	0.3	0.8	2.4
	.36	0	0	0	0	0	.2	.5	1.1	1.7
	.71	--	.2	.1	0	0	.1	.3	.6	1.1
	1.07	.6	.5	.4	.2	0	-.2	-.3	-.4	-.4
	1.43	--	.4	.3	.2	0	-.2	-.3	-.4	-.6
1.14	0	-.8	-.6	-.5	-.2	0	.3	.8	1.5	2.5
	.36	-.4	-.4	-.3	-.2	0	.3	.6	1.4	2.5
	.71	--	-.1	-.2	-.1	0	.2	.4	.7	1.3
	1.07	.4	.2	.1	0	0	-.1	-.3	-.6	-1.1
	1.43	--	.5	.4	.2	0	-.2	-.4	-.6	-.9
.86	0	-2.0	-1.4	-.8	-.2	0	.5	--	--	--
	.36	-.5	-.5	-.4	-.3	0	.4	1.2	2.3	--
	.71	-.2	-.2	-.2	-.2	0	.2	.5	1.0	1.6
	1.07	.3	.3	.2	.1	0	-.2	-.5	-1.0	-1.6
	1.43	.7	.6	.4	.3	0	-.3	-.6	-1.0	-1.5
.57	0	-2.0	-1.9	-1.5	-.8	0	.9	--	--	--
	.36	-1.1	-1.1	-.9	-.5	0	.6	--	--	--
	.71	-.6	-.6	-.5	-.4	0	.5	1.0	1.5	2.0
	1.07	-.2	-.2	0	.2	0	-.3	-1.0	-2.5	--
	1.43	.6	.5	.4	.2	0	-.4	-.9	-1.5	--
.29	.36	-1.2	-1.4	-1.3	-.8	0	.9	2.1	3.4	4.5
	.71	-.7	-.7	-.7	-.5	0	--	--	--	--
	1.07	.4	.4	.4	.3	0	-1.0	-3.0	-3.6	--
	1.43	--	1.1	.8	.5	0	-.5	-1.1	-1.9	-2.9
0	.36	-1.3	-1.5	-1.6	-1.3	0	1.0	1.7	2.0	1.7
	.71	-.8	-.8	-.7	-.4	0	.6	.9	.9	.9
	1.07	1.1	1.2	1.3	1.0	0	-1.1	-1.5	-1.7	-1.6
	1.43	1.5	1.4	1.2	.9	0	-.6	-1.0	-1.3	-1.5
-.29	.36	-5.4	-4.2	-2.6	-1.3	0	0.8	1.1	1.2	1.4
	.71	--	--	--	--	--	--	--	--	--
	1.07	--	--	--	--	--	--	--	--	--
	1.43	--	--	--	--	--	--	--	--	--
-.57	.36	--	--	--	-.8	0	.6	1.0	1.2	1.4
	.71	--	-1.8	-1.1	-.5	0	.3	.5	.6	.7
	1.07	--	4.1	1.9	.6	0	-.2	-.3	-.4	-.5
	1.43	--	1.5	.9	.4	0	-.3	-.5	-.6	--
-.86	.36	--	--	--	--	--	--	--	--	--
	.71	-1.6	-1.1	-.6	-.2	0	.2	.2	.3	.3
	1.07	--	1.5	.6	.2	0	-.2	-.3	-.4	-.5
	1.43	--	2.0	1.1	.4	0	-.2	-.3	-.4	-.5
-1.14	.36	--	-1.3	-.5	-.2	0	.2	.4	.5	.5
	.71	-.8	-.5	-.2	0	0	.1	.1	.1	.1
	1.07	.8	.6	.4	.3	0	-.2	-.3	-.3	-.3
	1.43	--	.7	.4	.3	0	-.2	-.3	-.4	-.4
-1.43	.36	-1.6	-1.0	-.5	-.1	0	.1	.1	.1	.1
	.71	-.6	-.4	-.2	-.1	0	0	0	0	0
	1.07	.1	.1	.2	.2	0	-.1	-.2	-.3	-.4
	1.43	.5	.3	.2	.1	0	-.1	-.2	-.4	-.6

TABLE I- CONTINUED

(a) $\varphi=0^\circ$ (Concluded).

$\frac{z}{s}$	$\frac{y}{s}$	σ', degrees								
		$\alpha=-8^\circ$	-6°	-4°	-2°	0°	2°	4°	6°	8°
1.43	1.43	0.8	0.6	0.4	0.2	0	-0.3	-0.6	-1.0	-1.4
	1.14	.3	.2	.2	.1	0	-.2	-.4	-.7	-1.1
	.86	.4	.3	.2	.1	0	-.2	-.4	-.7	-1.2
	.57	.1	.1	.1	.1	0	-.2	-.4	-.7	-1.2
	.29	--	--	--	--	--	--	--	--	--
	0	.1	.2	.2	.2	0	0	.1	.3	.5
	-.29	.3	.2	.1	.1	0	0	-.1	.2	.6
	-.57	-.1	-.2	-.1	0	0	0	.2	.7	1.2
	-.86	-.3	-.2	-.2	-.1	0	.1	.3	.7	1.2
	-1.14	-.3	-.2	-.1	-.1	0	.1	.4	.7	1.0
	-1.43	--	--	--	--	--	--	--	--	--
1.07	1.43	.7	.5	.3	.2	0	-.1	-.5	-.9	-1.2
	1.14	.4	.4	.4	.2	0	-.3	-.7	-1.3	-1.9
	.86	.6	.6	.5	.3	0	-.2	-.7	-1.5	-2.6
	.57	.5	.4	.4	.2	0	-.5	-.7	-1.3	-2.2
	.29	--	--	--	--	--	--	--	--	--
	0	-.2	-.1	0	0	0	.1	0	0	.1
	-.29	-.6	-.4	-.3	-.1	0	0	.2	.7	1.2
	-.57	-.6	-.5	-.4	-.2	0	.2	.7	1.4	2.3
	-.86	-.7	-.6	-.5	-.3	0	.4	.8	1.4	2.4
	-1.14	-.5	-.4	-.3	-.1	0	.3	.7	1.3	1.9
	-1.43	-.7	-.5	-.4	-.3	0	-.1	-.3	-.6	-1.0
.71	1.43	1.0	.9	.8	.5	0	-.4	-.8	-1.2	-1.5
	1.14	1.0	.9	.8	.6	0	-.7	-1.4	-2.0	-2.5
	.86	1.3	1.1	.9	.5	0	-.5	-1.4	-2.9	-4.9
	.57	.9	1.0	.8	.4	0	-.6	-1.5	-3.0	-5.4
	.29	--	--	--	--	--	--	--	--	--
	0	-.4	-.2	-.1	0	0	0	.1	.3	.4
	-.29	-.7	-.5	-.4	-.3	0	.2	.6	1.2	2.0
	-.57	-1.2	-1.0	-.8	-.4	0	.4	1.2	2.7	5.2
	-.86	-1.2	-.9	-.7	-.4	0	.5	1.4	2.8	4.8
	-1.14	-1.1	-1.0	-.7	-.4	0	.6	1.2	1.7	2.1
	-1.43	-.8	-.7	-.5	-.3	0	.4	.7	.9	1.2
.36	1.43	1.2	1.0	.7	.4	0	-.4	-.6	-.6	-.4
	1.14	2.1	1.8	1.5	.9	0	-.8	-1.2	-1.2	0
	.86	1.9	1.6	1.3	.7	0	--	--	--	--
	.57	1.7	1.6	1.3	.8	0	-1.0	-1.9	-1.1	1.6
	.29	--	--	--	--	--	--	--	--	--
	0	--	--	--	--	--	--	--	--	--
	-.29	-1.5	-1.2	-.9	-.5	0	.5	1.0	1.3	1.1
	-.57	-1.7	-1.7	-1.2	-.8	0	1.2	2.2	2.6	0
	-.86	-1.9	-1.6	-1.2	-.7	0	1.1	4.1	--	--
	-1.14	-1.6	-1.3	-1.0	-.5	0	.4	.8	.6	.7
	-1.43	-1.1	-.9	-.6	-.2	0	.4	.5	.5	.4
0	-.86	-3.2	-2.9	-2.4	-1.8	0	-.6	-2.6	-3.8	-3.6
	-1.14	-2.6	-2.1	-1.5	-.7	0	-.5	-1.3	-2.1	-2.7
	-1.43	-1.1	-.7	-.4	-.2	0	-.2	-.3	-.7	-1.0

TABLE I.- CONTINUED

(b) $\Phi = 11-1/4^\circ$.

$\frac{z}{s}$	$\frac{y}{s}$	ϵ', degrees								
		$\alpha=-8^\circ$	-6°	-4°	-2°	0°	2°	4°	6°	8°
1.43	0	-0.2	-0.2	-0.2	-0.2	0	0.2	0.7	1.4	2.4
	.36	-.4	-.2	-.1	0	0	.1	.4	.8	1.8
	.71	.4	.1	0	0	0	.1	.4	.9	1.4
	1.07	.8	.6	.4	.2	0	-.2	-.4	-.5	-.5
	1.43	1.0	.7	.5	.3	0	-.3	-.5	-.6	-.6
1.14	0	-.8	-.6	-.4	-.2	0	.5	--	--	--
	.36	-.6	-.5	-.1	0	0	.1	.3	.9	2.0
	.71	0	0	0	0	0	0	.2	.5	1.0
	1.07	-.1	-.1	0	0	0	-.2	-.3	-.4	-.5
	1.43	.9	.6	.4	.2	0	-.1	-.2	-.4	-.6
.86	0	-1.6	-1.3	-1.0	-.6	0	.8	--	--	--
	.36	-.6	-.1	0	0	0	.2	.7	1.6	--
	.71	0	.1	.1	.1	0	-.1	-.1	.4	1.1
	1.07	--	-.1	0	0	0	-.2	-.4	-.5	-.9
	1.43	.6	.5	.4	.2	0	-.2	-.6	-1.0	-1.4
.57	0	-3.4	-2.8	-2.0	-1.0	0	1.1	--	--	--
	.36	--	.2	-.3	-.2	0	.4	1.1	--	--
	.71	-.2	-.2	-.2	-.1	0	0	.5	1.3	2.3
	1.07	-.3	-.1	0	0	0	-.2	-.4	-1.3	-2.6
	1.43	.6	.5	.5	.4	0	-.3	-.7	-1.3	-2.0
.29	.36	-.5	-.7	-.6	-.5	0	.8	1.8	--	--
	.71	.4	.1	0	0	0	.2	.9	--	--
	1.07	.2	.4	.4	.3	0	-.7	-2.3	-4.5	--
	1.43	.4	.3	.3	.2	0	-.9	-1.8	-2.5	-2.8
0	.36	-1.0	-1.1	-1.2	-.9	0	1.0	1.9	2.4	2.6
	.71	-.4	-.6	-.6	-.5	0	.5	1.7	1.1	.7
	1.07	.4	.4	.7	.6	0	-1.2	-2.4	-2.6	-2.3
	1.43	1.0	.9	.8	.5	0	-.8	-1.4	-1.8	-2.2
-.29	.36	-3.2	-3.7	-2.8	-1.0	0	.9	1.5	1.9	2.2
	.71	-2.4	-3.4	-3.3	-1.0	0	.1	.1	.1	.2
	1.07	--	--	--	--	-	--	--	--	--
	1.43	--	--	--	--	-	--	--	--	--
-.57	.36	--	--	--	--	0	1.1	1.8	2.2	2.5
	.71	--	--	--	-.7	0	.3	.5	.7	.8
	1.07	--	4.4	3.1	1.0	0	-.3	-.5	-.5	-.5
	1.43	2.0	1.6	1.0	.4	0	-.6	-1.1	1.4	1.5
-.86	.36	--	--	--	--	-	--	--	--	--
	.71	-1.8	-1.0	-.5	-.2	0	.3	.5	.6	--
	1.07	3.8	2.2	1.0	.2	0	-.2	-.4	-.4	-.4
	1.43	2.2	1.5	1.0	.4	0	-.5	-.7	-.9	-1.0
-1.14	.36	-3.2	-2.0	-1.1	-.5	0	.3	.5	.6	.7
	.71	-1.0	-.6	-.2	-.1	0	0	0	0	0
	1.07	.9	.6	.3	.2	0	-.1	-.1	-.2	-.2
	1.43	1.2	.8	.4	.2	0	-.3	-.5	-.5	-.6
-1.43	.36	-2.1	-1.3	-.8	-.3	0	.2	.3	.4	.5
	.71	-2.0	-.9	-.4	0	0	0	0	-.1	-.2
	1.07	-.1	0	.1	.1	0	-.2	-.2	-.2	-.1
	1.43	.6	.5	.5	.3	0	-.2	-.3	-.4	-.4

TABLE I.- CONTINUED

(b) φ=11-1/4° (Concluded).

$\frac{z}{s}$	$\frac{y}{s}$	σ', degrees								
		α=-8°	-6°	-4°	-2°	0°	2°	4°	6°	8°
1.43	1.43	0.8	0.6	0.4	0.2	0	-0.1	-0.3	-0.6	-0.9
	1.14	.3	.3	.2	.1	0	-.1	-.4	-.6	-.9
	.86	.3	.3	.3	.2	0	-.1	-.4	-.7	-1.2
	.57	.3	.3	.3	.2	0	-.2	-.3	-.6	-1.0
	.29	--	--	--	--	--	--	--	--	--
	0	.4	.2	.1	.1	0	0	-.1	-.1	-.2
	-.29	0	0	0	0	0	0	0	0	.2
	-.57	-.1	-.1	-.1	0	0	0	.4	.9	1.5
	-.86	-.5	-.3	0	0	0	.1	.4	.8	1.4
	-1.14	-.6	-.5	-.3	-.1	0	.2	.4	.7	1.1
	-1.43	--	--	--	--	--	--	--	--	--
1.07	1.43	.5	.4	.3	.2	0	-.1	-.6	-1.0	-1.3
	1.14	.4	.4	.4	.2	0	-.3	-.7	-1.2	-1.7
	.86	.9	.7	.5	.3	0	-.4	-.8	-1.5	-2.3
	.57	.7	.6	.5	.3	0	-.3	-.6	-1.3	-1.7
	.29	--	--	--	--	--	--	--	--	--
	0	.1	.2	.3	.2	0	-.1	-.1	.3	.9
	-.29	-.4	-.5	-.2	0	0	0	.3	.8	1.6
	-.57	-.5	-.4	-.3	-.2	0	.3	.9	1.8	3.1
	-.86	-.9	-.8	-.6	-.3	0	.3	.8	1.7	2.9
	-1.14	-.7	-.5	-.4	-.2	0	.4	.8	1.3	2.0
	-1.43	-.7	-.6	-.4	-.2	0	.3	.6	.9	1.2
.71	1.43	.9	.7	.6	.4	0	-.3	-.6	-1.0	-1.5
	1.14	1.0	.7	.6	.3	0	-.5	-1.0	-1.7	-2.6
	.86	1.1	.9	.7	.5	0	-.4	-1.1	-2.2	-3.8
	.57	1.0	.8	.6	.3	0	-.5	-1.0	-2.1	-3.9
	.29	--	--	--	--	--	--	--	--	--
	0	.1	0	0	0	0	0	.3	.8	1.0
	-.29	-.7	-.6	-.4	-.2	0	.2	.6	1.1	2.0
	-.57	-1.2	-1.1	-.9	-.5	0	.7	1.8	4.1	8.9
	-.86	-1.3	-1.1	-.8	-.5	0	.6	2.0	4.1	6.1
	-1.14	-1.5	-1.3	-.9	-.5	0	.4	.9	1.4	1.6
	-1.43	-1.0	-.7	-.5	-.2	0	.2	.4	.5	.5
.36	1.43	1.0	.8	.6	.4	0	-.4	-.8	-.9	-.9
	1.14	1.6	1.3	1.0	.5	0	-.8	-1.6	-2.1	-1.7
	.86	1.2	1.0	.7	.4	0	-.4	-1.2	-3.0	--
	.57	1.1	1.0	.8	.6	0	-.9	-1.9	-3.3	-1.6
	.29	--	--	--	--	--	--	--	--	--
	0	--	--	--	--	--	--	--	--	--
	-.29	-2.0	-1.5	-1.0	-.6	0	.6	1.2	1.1	.5
	-.57	-2.3	-2.0	-1.6	-.9	0	1.3	2.1	.3	-1.6
	-.86	-2.2	-2.0	-1.6	-1.0	0	2.3	-1.5	-5.9	--
	-1.14	-1.9	-1.5	-1.1	-.6	0	.4	.2	-.4	-1.5
	-1.43	-1.1	-.8	-.6	-.4	0	.2	.2	0	-.4
0	-.86	-7.7	-6.8	-5.9	-3.6	0	-2.1	-3.0	-3.6	-4.0
	-1.14	-3.3	-2.6	-1.4	-.4	0	-.4	-1.0	-1.6	-2.1
	-1.43	-1.1	-.7	-.2	0	0	-.1	-.3	-.6	-1.0

TABLE I.- CONTINUED

(c) Φ=22-1/2°.

$\frac{z}{s}$	$\frac{y}{s}$	ϵ', degrees								
		α=-8°	-6°	-4°	-2°	0°	2°	4°	6°	8°
1.43	0	-0.5	-0.6	-0.5	-0.3	0	0.3	0.8	1.5	2.5
	.36	0	0	0	0	0	.1	.4	1.1	1.2
	.71	.2	.1	0	0	0	.1	.2	.4	.6
	1.07	1.2	.7	.4	.1	0	-.2	-.3	-.3	-.4
	1.43	1.6	1.1	.7	.4	0	-.2	-.4	-.5	-.5
1.14	0	-1.0	-.9	-.7	-.5	0	.6	1.5	--	--
	.36	-.5	-.4	-.3	-.2	0	0	.2	-1.4	-1.3
	.71	.1	.2	.3	.3	0	-.1	-.1	-.1	.1
	1.07	.5	.4	.2	.1	0	-.3	-.3	-.5	-.5
	1.43	1.7	.9	.7	.6	0	-.3	-.4	-.5	-.5
.86	0	-2.1	-1.8	-1.4	-.8	0	1.0	2.1	--	--
	.36	-.8	-.7	-.5	-.3	0	-.2	-.1	.6	--
	.71	.3	.6	.6	.5	0	-.3	-.3	-.2	.2
	1.07	.5	.5	.4	.3	0	-.3	-.5	-.6	-.7
	1.43	.6	.6	.5	.4	0	-.4	-.6	-.8	-1.0
.57	0	-3.9	-3.0	-2.0	-1.1	0	1.2	2.8	--	--
	.36	-3.0	-1.5	-.3	.5	0	.3	1.0	2.0	--
	.71	1.0	1.0	.8	.5	0	-.4	-.2	.3	--
	1.07	.5	.4	.3	.1	0	-.2	-.4	-.8	-1.8
	1.43	.7	.6	.5	.3	0	-.3	-.7	-1.1	-1.6
.29	.36	--	-.5	-.4	-.2	0	.4	1.3	2.7	--
	.71	2.0	1.1	.5	.2	0	.1	.2	1.0	2.2
	1.07	1.0	.7	.5	.2	0	-.4	-1.1	-2.7	--
	1.43	.9	.8	.6	.4	0	-.5	-1.2	-2.1	-3.0
0	.36	-.7	-.7	-.6	-.4	0	.7	2.6	3.9	4.3
	.71	.6	.2	.1	0	0	.1	1.0	--	4.5
	1.07	1.0	.8	.5	.3	0	-.5	-2.3	-3.7	--
	1.43	1.1	.8	.6	.4	0	-.7	-1.2	-1.8	-2.3
-0.29	0.36	-2.0	-2.6	-2.5	-1.3	0	1.2	2.1	2.6	2.9
	.71	-.3	-.3	-.3	-.2	0	.2	.2	.2	.3
	1.07	--	--	--	--	-	--	--	--	--
	1.43	--	--	--	--	-	--	--	--	--
-.57	.36	-6.2	-5.6	-3.0	-1.6	0	.9	1.7	2.3	2.5
	.71	.4	.5	-6.0	-2.5	0	.4	.6	.8	.9
	1.07	2.5	2.5	2.1	1.2	0	-.7	-1.0	-1.2	-1.3
	1.43	1.9	1.5	1.1	.8	0	-.7	-1.0	-1.2	-1.3
-.86	.36	--	--	--	--	-	--	--	--	--
	.71	1.0	.9	-.6	-.5	0	.4	.7	.8	1.0
	1.07	--	3.2	1.6	.6	0	-.3	-.5	-.5	-.6
	1.43	2.0	1.5	1.1	.6	0	-.4	-.6	-.8	-1.0
-1.14	.36	--	--	--	-.5	0	.3	.8	.8	.9
	.71	-.5	-.4	-.1	0	0	0	0	0	0
	1.07	--	--	--	--	-	--	--	--	--
	1.43	1.6	1.0	.6	.4	0	.3	.4	.5	.6
-1.43	.36	--	-1.5	-.7	-.3	0	.2	.4	.6	.7
	.71	-.4	-.1	0	0	0	0	0	0	0
	1.07	.5	.3	.2	.1	0	0	0	0	0
	1.43	.8	.7	.5	.3	0	0	-.1	-.3	-.5

TABLE I.- CONTINUED

(c) $\varphi=22-1/2^{\circ}$ (Concluded).

$\frac{z}{s}$	$\frac{y}{s}$	σ', degrees								
		$\alpha=-8^{\circ}$	-6°	-4°	-2°	0°	2°	4°	6°	8°
1.43	1.43	0.6	0.5	0.4	0.3	0	-0.2	-0.4	-0.6	-0.8
	1.14	-.1	0	.1	.1	0	-.2	-.4	-.6	-.9
	.86	.5	.6	.5	.3	0	-.2	-.5	-.8	-1.2
	.57	.7	.7	.6	.4	0	-.1	-.4	-.8	-1.3
	.29	--	--	--	--	--	--	--	--	--
	0	.4	.5	.4	.2	0	-.1	-.2	-.2	-.2
	-.29	-.1	0	0	0	0	-.1	-.1	.1	.3
	-.57	-.3	-.2	-.1	0	0	.1	.4	.9	1.7
	-.86	-.6	-.4	-.2	-.1	0	.1	.4	.8	1.6
	-1.14	-.7	-.6	-.5	-.3	0	.2	.5	.8	1.2
	-1.43	--	--	--	--	--	--	--	--	--
1.07	1.43	-.1	-.1	0	0	0	-.3	-.6	-.9	-1.1
	1.14	.6	.6	.5	.3	0	-.2	-.5	-.8	-1.2
	.86	1.1	.8	.6	.3	0	-.3	-.6	-1.1	-1.6
	.57	1.3	1.1	.9	.7	0	-.4	-.7	-1.1	-1.5
	.29	--	--	--	--	--	--	--	--	--
	0	.1	.1	.1	0	0	-.1	0	.4	1.0
	-.29	-.4	-.4	-.3	-.1	0	0	.4	1.0	1.9
	-.57	-.8	-.8	-.6	-.4	0	.4	1.1	2.3	4.1
	-.86	-1.1	-.9	-.7	-.4	0	.5	1.1	2.1	3.2
	-1.14	-1.0	-.8	-.6	-.3	0	.3	.8	1.5	2.1
	-1.43	-1.0	-.7	-.5	-.3	0	.2	.4	.7	.9
.71	1.43	.8	.9	.7	.4	0	-.3	-.6	-1.0	-1.3
	1.14	1.0	.8	.7	.4	0	-.4	-.7	-1.2	-2.0
	.86	1.7	1.4	1.0	.5	0	-.2	-.6	-1.1	-2.1
	.57	2.6	2.1	1.4	.6	0	-.3	-.6	-1.2	-2.1
	.29	--	--	--	--	--	--	--	--	--
	0	0	0	0	0	0	.1	.3	.6	.7
	-.29	-.8	-.7	-.5	-.2	0	.2	.7	1.2	1.5
	-.57	-1.6	-1.4	-1.2	-.7	0	.9	2.3	8.0	7.1
	-.86	-1.5	-1.3	-1.0	-.6	0	.9	2.7	3.5	3.0
	-1.14	-1.7	-1.4	-.9	-.5	0	.3	.6	.6	.1
	-1.43	-1.0	-.7	-.4	-.2	0	.2	.3	.3	.3
.36	1.43	.9	.8	.6	.3	0	-.3	-.6	-.9	-1.1
	1.14	1.2	.9	.7	.4	0	-.6	-1.1	-1.7	-2.1
	.86	1.0	.8	.5	.3	0	-.5	-1.4	-2.9	-5.4
	.57	-.4	-.1	.3	.3	0	-.4	-1.1	-2.4	-5.1
	.29	--	--	--	--	--	--	--	--	--
	0	--	--	--	--	--	--	--	--	--
	-.29	-2.0	-1.6	-1.2	-.7	0	.6	.9	.5	-.3
	-.57	-2.9	-2.7	-2.2	-1.3	0	1.3	1.3	-.4	-2.1
	-.86	-2.7	-2.7	-2.3	-1.5	0	-.5	-1.7	-2.5	-2.7
	-1.14	-2.6	-2.0	-1.4	-.8	0	-.2	-.6	-1.1	-1.5
	-1.43	-1.3	-.9	-.5	-.1	0	-.1	-.2	-.4	-.6
0	-.86	--	--	1.1	3.9	0	-.8	-1.4	-1.7	-1.8
	-1.14	-2.8	-1.3	0	.5	0	-.5	-1.0	-1.3	-1.5
	-1.43	-.5	-.1	.2	.3	0	-.3	-.6	-.9	-1.1

TABLE I.- CONTINUED

(d) $\varphi=45^\circ$.

$\frac{z}{s}$	$\frac{y}{s}$	ϵ', degrees								
		$\alpha=-8^\circ$	-6°	-4°	-2°	0°	2°	4°	6°	8°
1.43	0	-0.8	-0.9	-0.8	-0.5	0	0.5	1.2	1.9	2.7
	.36	-.7	-.7	-.5	-.3	0	.4	.9	1.5	2.2
	.71	-.3	-.4	-.3	-.2	0	.2	.2	.1	- -
	1.07	.3	.3	.3	.2	0	-.4	-.5	-.7	-.8
	1.43	.6	.5	.4	.3	0	-.4	-.6	-.8	-.9
1.14	0	- -	-1.4	-1.1	-.6	0	.6	- -	- -	- -
	.36	-1.0	-.9	-.7	-.4	0	.5	- -	- -	- -
	.71	-.4	-.3	-.2	0	0	-.1	-.2	-.7	-2.0
	1.07	.2	.2	.2	.1	0	-.4	-.6	-1.0	-1.2
	1.43	1.3	1.0	.7	.4	0	-.3	-.6	-.8	-1.1
.86	0	-2.5	-2.1	-1.7	-1.2	0	- -	- -	- -	- -
	.36	-1.5	-1.3	-1.1	-.6	0	.9	2.8	5.2	6.9
	.71	-.3	-.2	0	0	0	-.7	-2.2	-2.7	-2.3
	1.07	.4	.5	.5	.5	0	-.5	-.9	-1.2	-1.4
	1.43	1.0	.8	.6	.3	0	-.4	-.7	-1.0	-1.2
.57	0	-3.7	-3.1	-2.3	-1.3	0	1.3	2.7	- -	- -
	.36	-3.2	-3.1	-2.7	-1.5	0	1.4	2.8	3.5	3.7
	.71	- -	-.5	-.2	- -	0	-.7	-.9	-1.1	- -
	1.07	.8	1.0	1.0	.8	0	-.5	-.8	-1.0	-1.2
	1.43	1.2	1.1	.9	.5	0	-.5	-.8	-1.0	-1.1
.29	.36	-5.3	-4.8	-3.6	-1.5	0	.8	1.3	2.4	- -
	.71	- -	- -	- -	.7	0	-.3	-.5	-.5	-.5
	1.07	2.4	2.1	1.6	.9	0	-.5	-.8	-1.2	-1.9
	1.43	1.7	1.4	1.1	.6	0	-.4	-.8	-1.1	-1.5
0	.36	- -	-2.7	1.2	-.5	0	.5	- -	- -	- -
	.71	- -	1.0	0	0	0	0	-.1	-.3	- -
	1.07	2.9	1.8	1.0	.4	0	-.3	-.8	-1.4	-2.6
	1.43	1.7	1.3	.8	.4	0	-.4	-.8	-1.3	-1.5
-.29	.36	- -	- -	-1.5	-.9	0	1.4	2.9	4.3	4.9
	.71	1.5	.8	.4	.2	0	-.1	-.2	- -	- -
	1.07	- -	- -	- -	- -	-	- -	- -	- -	- -
	1.43	- -	- -	- -	- -	-	- -	- -	- -	- -
-.57	.36	-3.7	-3.5	-2.7	-1.5	0	1.6	2.6	3.2	3.6
	.71	.4	.7	.9	.8	0	-.4	-.2	-.1	-.2
	1.07	1.5	.9	.5	.2	0	-.3	-.9	-1.3	-1.5
	1.43	1.6	1.2	.8	.4	0	-.4	-.8	-1.1	-1.2
-.86	.36	- -	- -	- -	- -	-	- -	- -	- -	- -
	.71	2.7	2.9	3.1	1.8	0	-.1	-.1	0	.2
	1.07	1.5	1.3	1.1	.6	0	-.4	-.6	-.7	-.8
	1.43	1.6	1.3	.9	.5	0	-.2	-.5	-.7	-.9
-1.14	.36	- -	- -	-1.5	-.7	0	.5	.7	.8	.8
	.71	- -	2.4	1.1	.2	0	0	0	0	0
	1.07	1.2	1.0	.7	.4	0	-.2	-.3	-.4	-.4
	1.43	1.1	.9	.6	.4	0	-.3	-.6	-.8	-.9
-1.43	.36	-2.2	-1.5	-.9	-.4	0	.3	.4	.4	.4
	.71	.8	.4	.2	.1	0	0	0	0	0
	1.07	.7	.6	.5	.3	0	-.2	-.2	-.2	-.1
	1.43	.5	.5	.4	.2	0	-.3	-.5	-.6	-.5

TABLE I

(d) $\varphi=45^\circ$ (Concluded).

$\frac{z}{s}$	$\frac{y}{s}$	σ', degrees								
		$\alpha=-8^\circ$	-6°	-4°	-2°	0°	2°	4°	6°	8°
1.43	1.43	0.6	0.5	0.4	0.3	0	-.3	-.5	-.6	-.7
	1.14	.5	.5	.4	.2	0	-.2	-.5	-.8	-1.0
	.86	.7	.6	.5	.3	0	-.3	-.6	-1.1	-1.5
	.57	.6	.5	.4	.2	0	-.3	-.7	-1.2	-2.0
	.29	- -	- -	- -	- -	-	- -	- -	- -	- -
	0	0	0	0	0	0	0	0	.2	.5
	-.29	-.2	-.2	-.2	-.1	0	.1	.4	.8	1.4
	-.57	-.6	-.5	-.4	-.2	0	.2	.7	1.2	2.1
	-.86	-.8	-.6	-.4	-.2	0	.2	.6	1.1	1.6
	-1.14	-.5	-.5	-.4	-.3	0	.2	.5	.9	1.2
	-1.43	- -	- -	- -	- -	-	- -	- -	- -	- -
1.07	1.43	.6	.5	.3	.2	0	-.2	-.4	-.6	-.7
	1.14	.7	.7	.6	.4	0	-.3	-.6	-.9	-1.1
	.86	1.4	1.2	1.0	.6	0	-.6	-1.1	-1.6	-2.0
	.57	1.0	.9	.7	.4	0	-.7	-2.0	-3.8	-5.4
	.29	- -	- -	- -	- -	0	- -	- -	- -	- -
	0	0	0	0	0	0	.1	.2	.4	.6
	-.29	-.9	-.7	-.5	-.3	0	.2	.7	1.5	3.2
	-.57	-1.4	-1.2	-1.0	-.6	0	.6	1.8	3.7	5.7
	-.86	-1.4	-1.2	-1.0	-.6	0	.5	.9	1.3	1.5
	-1.14	-1.2	-1.0	-.8	-.4	0	.2	.5	.8	1.0
	-1.43	-.6	-.5	-.3	-.2	0	.2	.3	.4	.6
.71	1.43	1.1	.9	.7	.4	0	-.3	-.4	-.5	-.6
	1.14	1.7	1.3	.9	.4	0	-.4	-.6	-.7	-.8
	.86	2.6	2.3	1.8	1.0	0	-.4	-.3	-.1	0
	.57	2.5	2.3	2.0	1.3	0	-1.0	.5	1.7	1.8
	.29	- -	- -	- -	- -	-	- -	- -	- -	- -
	0	-.3	-.2	-.1	0	0	0	.1	.2	.3
	-.29	-1.4	-1.2	-.8	-.5	0	.2	.5	.1	-.8
	-.57	-2.4	-2.3	-1.9	-1.1	0	1.1	-.6	-1.7	-1.8
	-.86	-2.5	-2.2	-1.7	-1.0	0	.4	.3	.1	0
	-1.14	-1.9	-1.4	-.8	-.4	0	.2	.3	.4	.5
	-1.43	-1.0	-.7	-.3	-.1	0	.2	.4	.4	.5
.36	1.43	1.4	.9	.6	.2	0	-.1	-.2	-.3	-.5
	1.14	2.2	1.4	.8	.3	0	-.1	-.2	-.4	-.8
	.86	5.0	2.8	.5	-.2	0	.3	.2	-.1	- -
	.57	- -	3.4	-.7	-1.0	0	.4	.5	.4	-.5
	.29	- -	- -	- -	- -	-	- -	- -	- -	- -
	0	- -	- -	- -	- -	-	- -	- -	- -	- -
	-.29	-2.4	-1.8	-1.1	-.6	0	-.2	-.4	0	.7
	-.57	- -	-5.4	-.7	.9	0	-.8	-1.4	-1.3	-.6
	-.86	-5.5	-3.2	-.6	.4	0	-.4	-.6	-.6	.1
	-1.14	-1.6	-.8	-.3	-.1	0	-.1	-.2	-.1	0
	-1.43	-.6	-.3	-.1	0	0	0	0	.1	.2
0	-.86	3.0	2.3	1.2	.3	0	-.1	.2	.6	1.1
	-1.14	0	.2	.2	.1	0	-.1	-.2	-.1	0
	-1.43	.1	.2	.2	.2	0	-.1	-.1	-.1	-.1

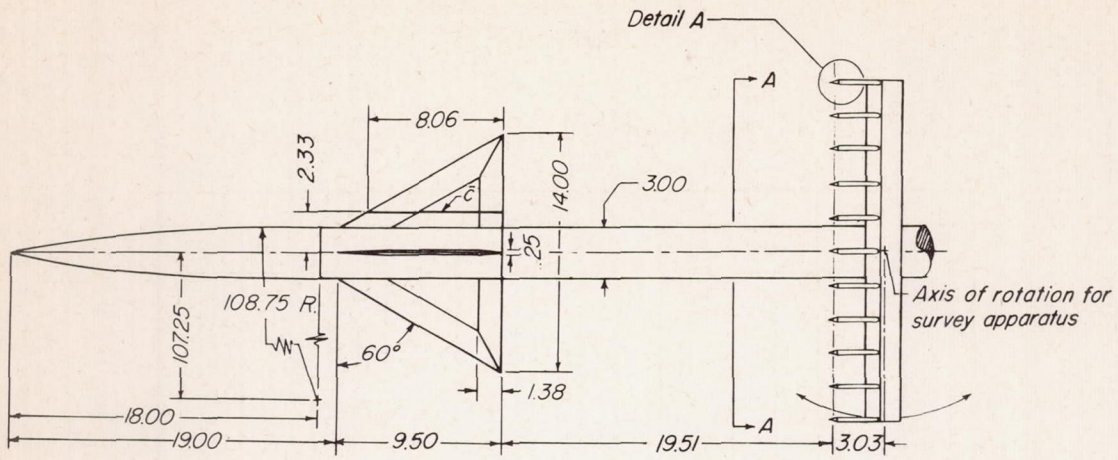

Side view of wing-body combination and survey apparatus

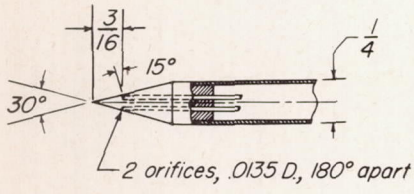

Detail A

30° cone

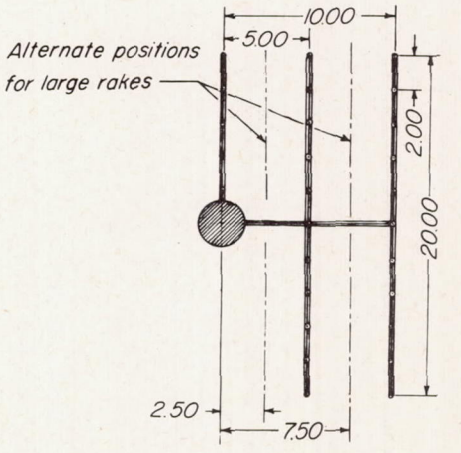

Section AA

Front view of survey apparatus

NACA

All dimensions are in inches

Figure 1. - Cruciform-wing and body combination and survey apparatus.

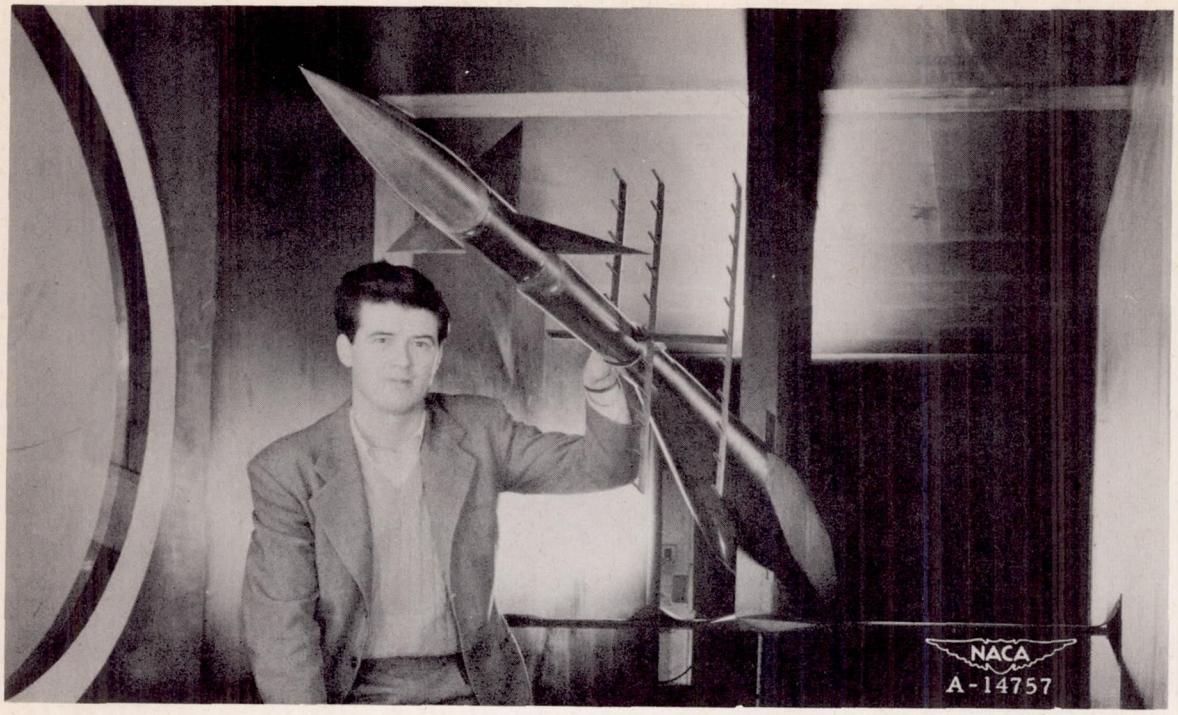

(a) Survey apparatus oriented for downwash measurements.

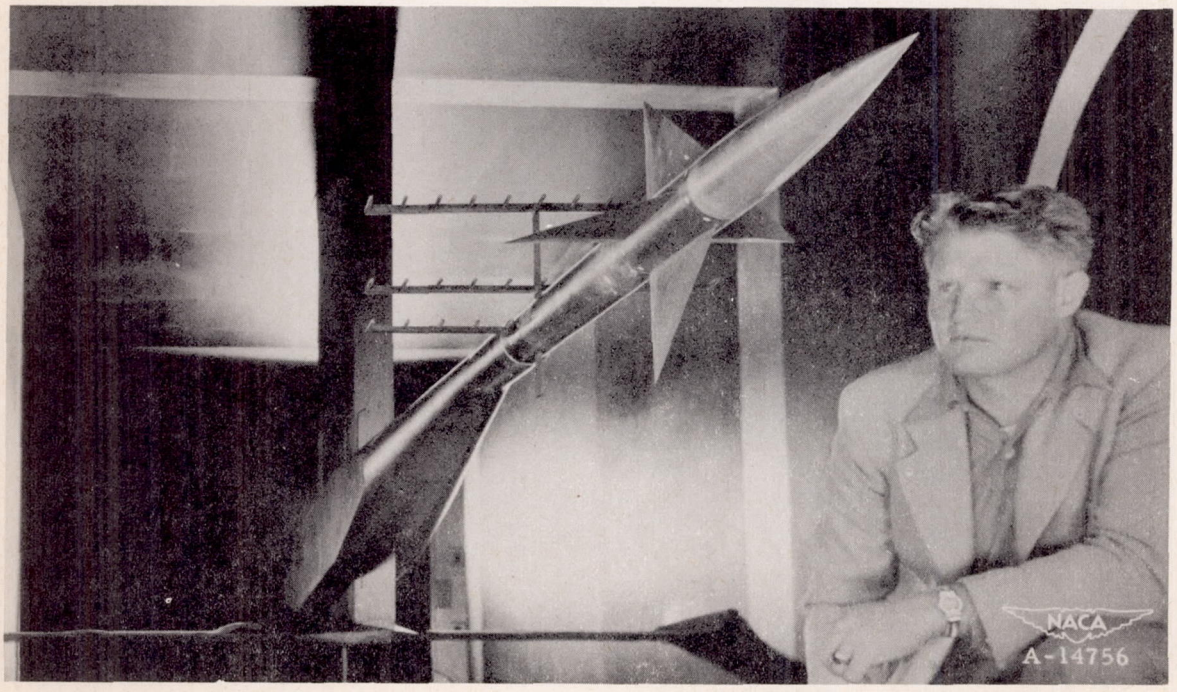

(b) Survey apparatus oriented for sidewash measurements.

Figure 2.- View of model and survey apparatus mounted in the Ames 6- by 6-foot supersonic wind tunnel.

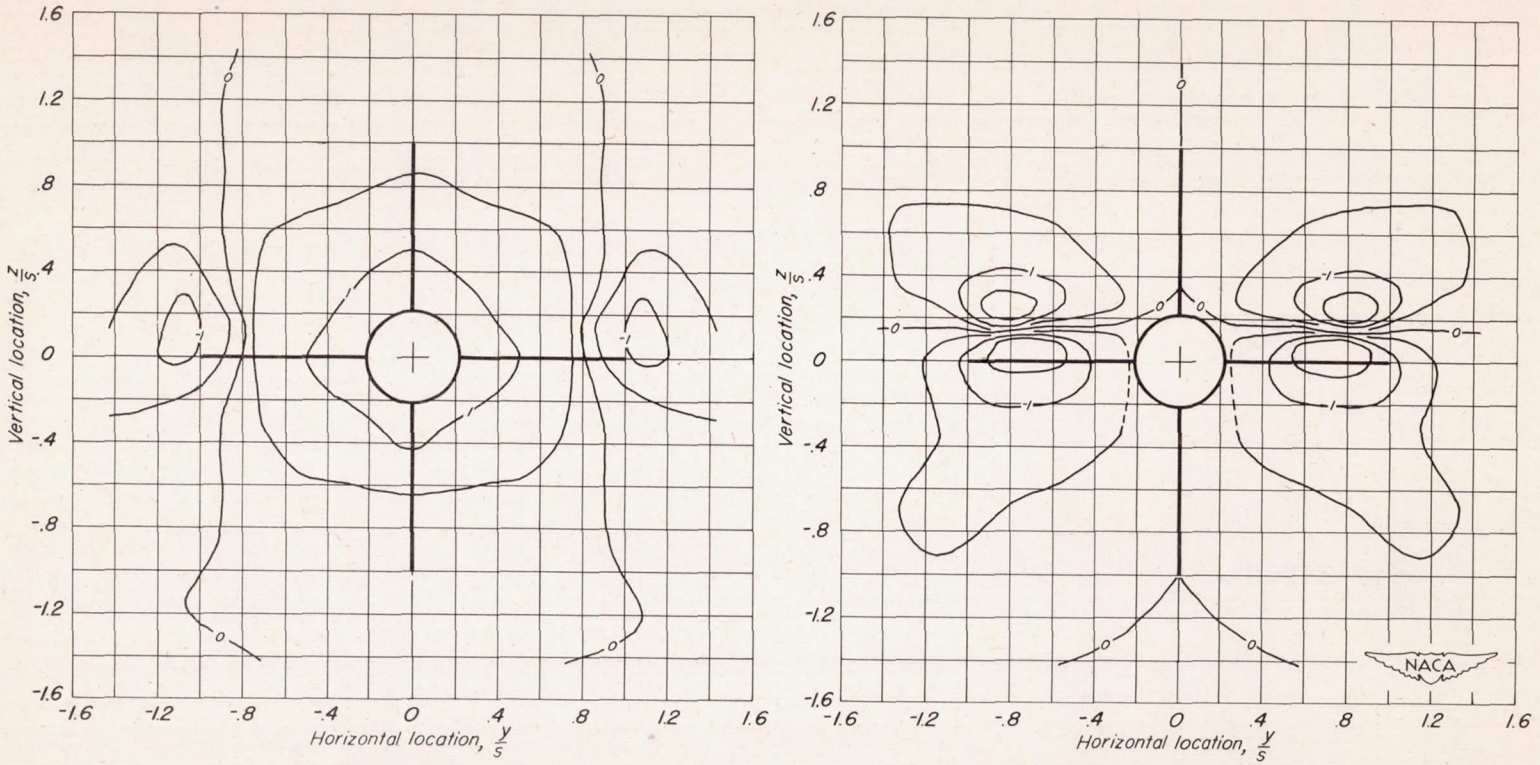

(a) $\alpha = 2°$

Figure 3.–Contours of constant angles of downwash and sidewash. $\phi = 0°$.

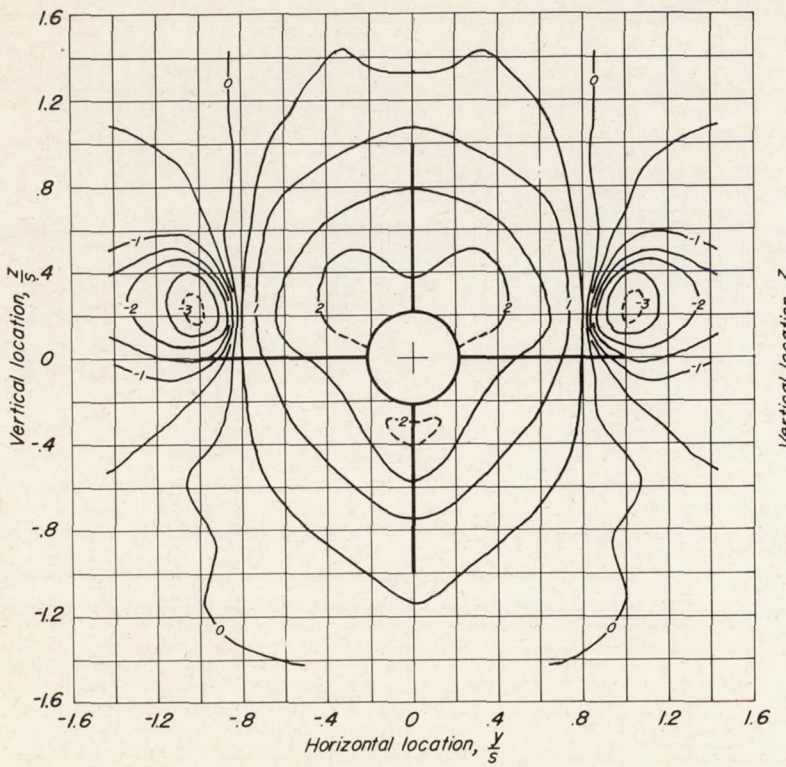

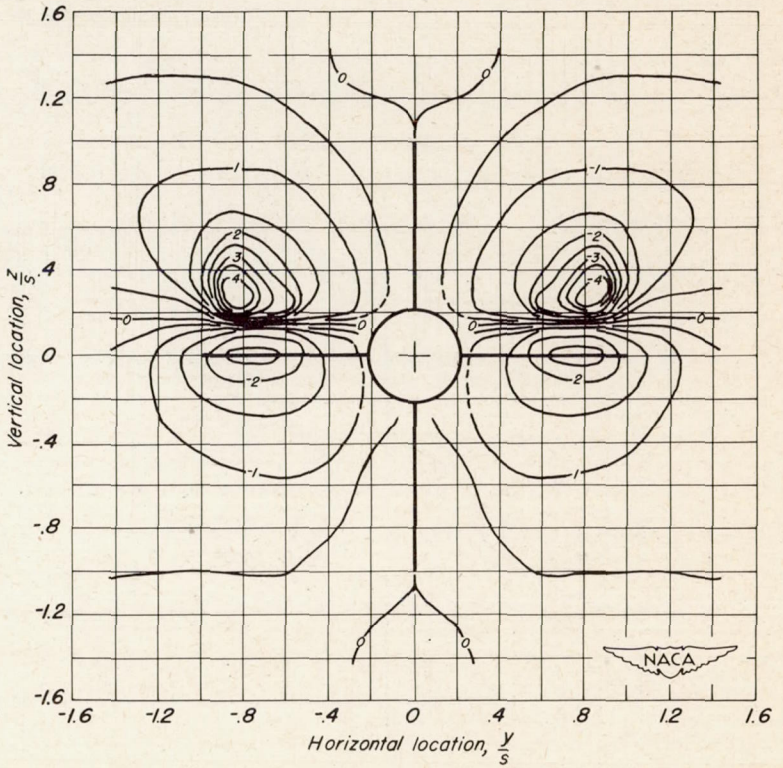

(b) $\alpha = 4°$

Figure 3.—Continued.

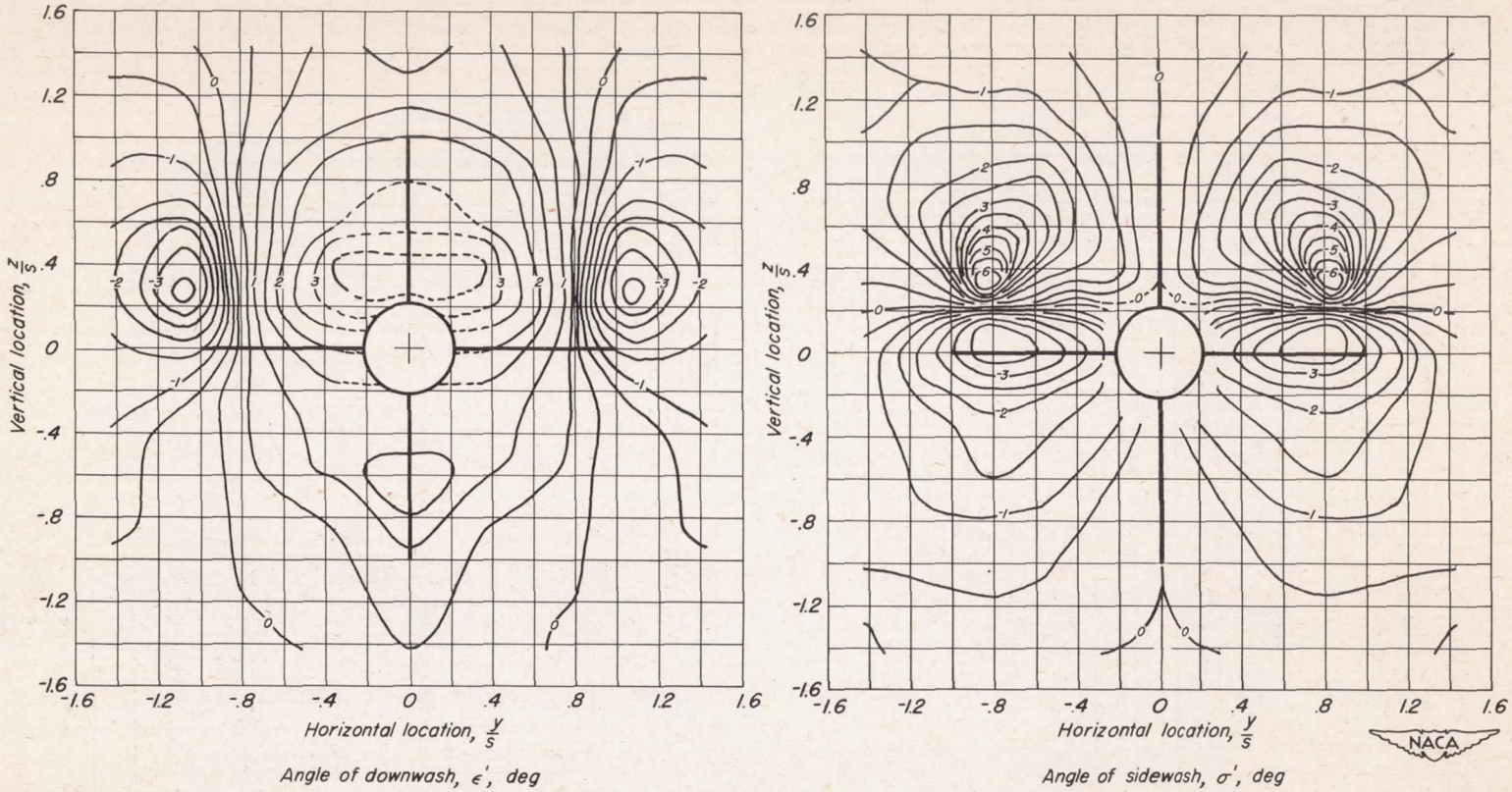

(c) $\alpha = 6°$

Figure 3.—Continued.

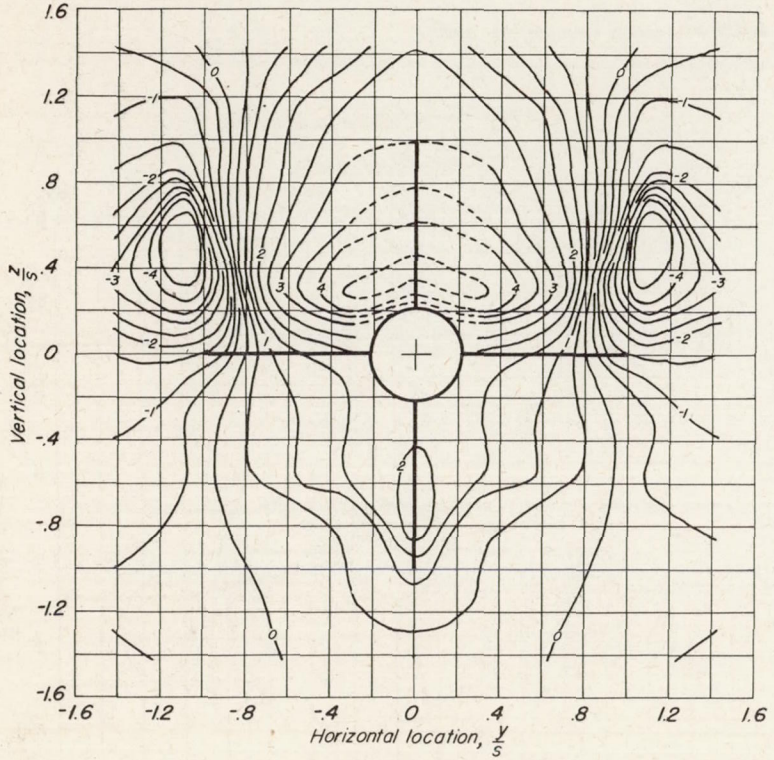

Angle of downwash, ϵ', deg

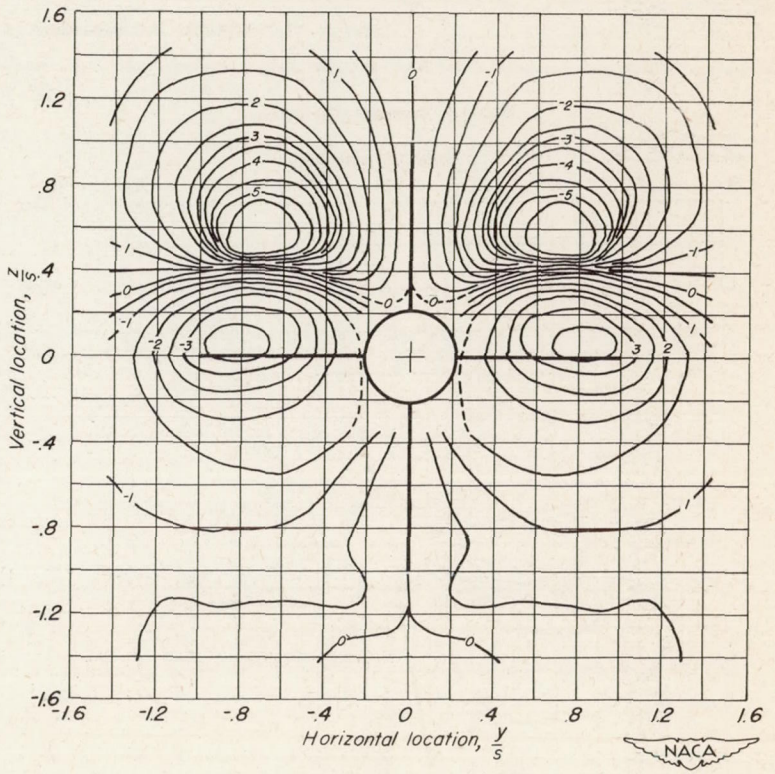

Angle of sidewash, σ', deg

(d) $\alpha = 8°$

Figure 3.—Concluded.

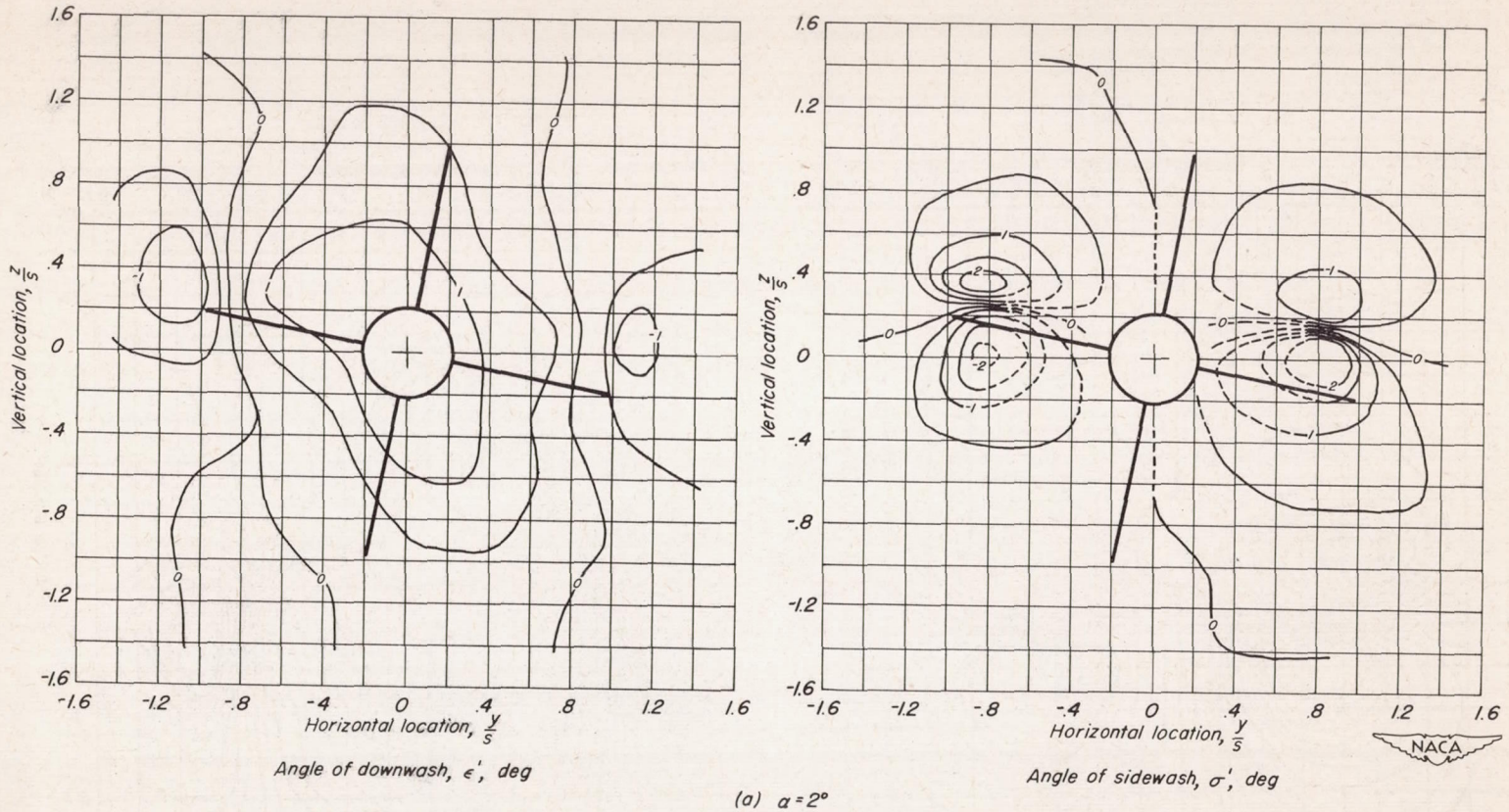

(a) $\alpha = 2°$

Figure 4.—Contours of constant angles of downwash and sidewash. $\phi = 11\text{-}1/4°$.

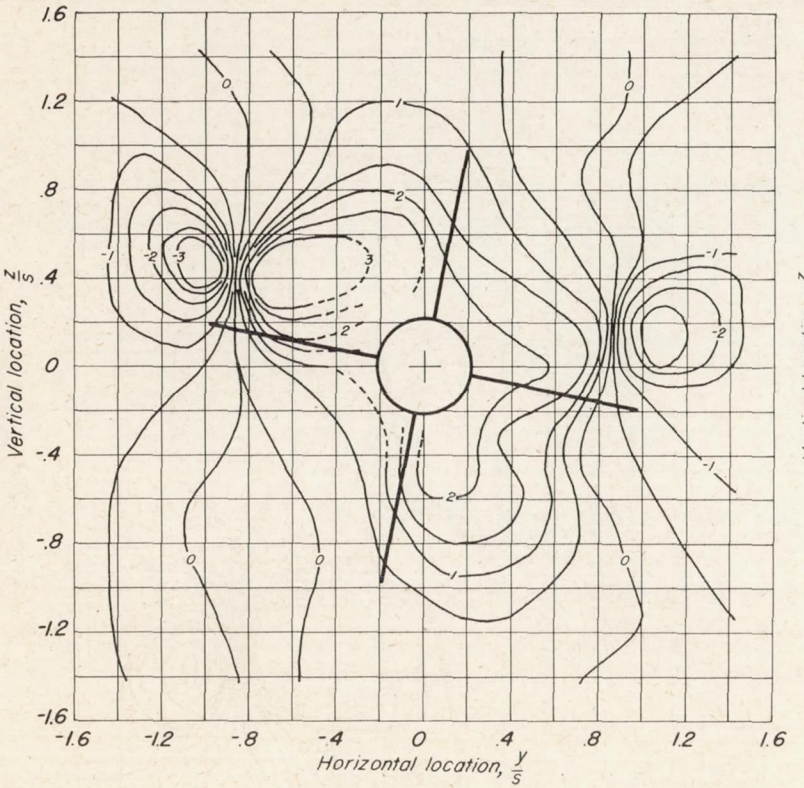

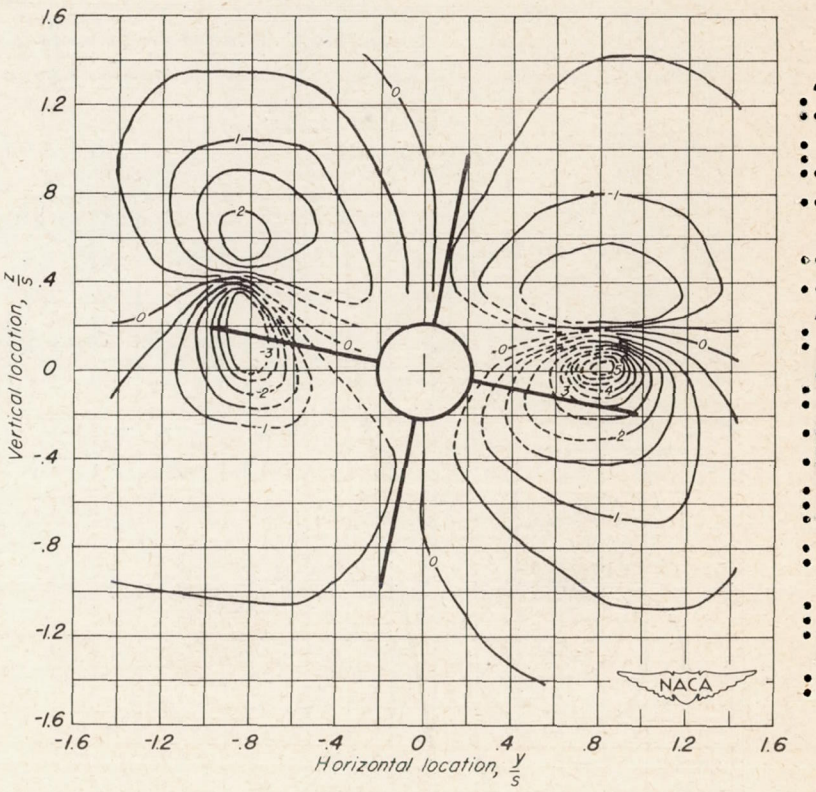

(b) $\alpha = 4°$

Figure 4.—Continued.

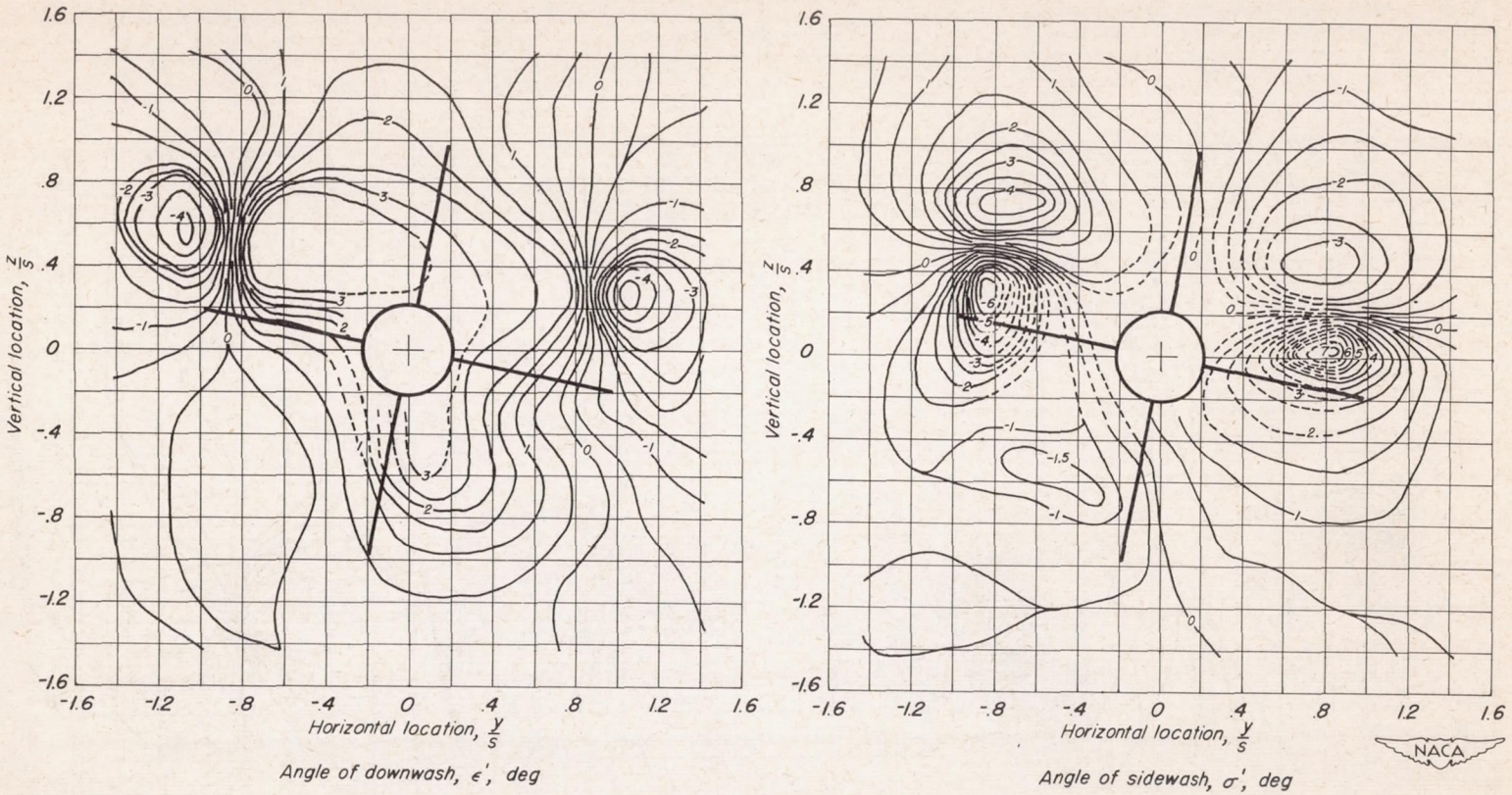

(c) $\alpha = 6°$

Figure 4.—Continued.

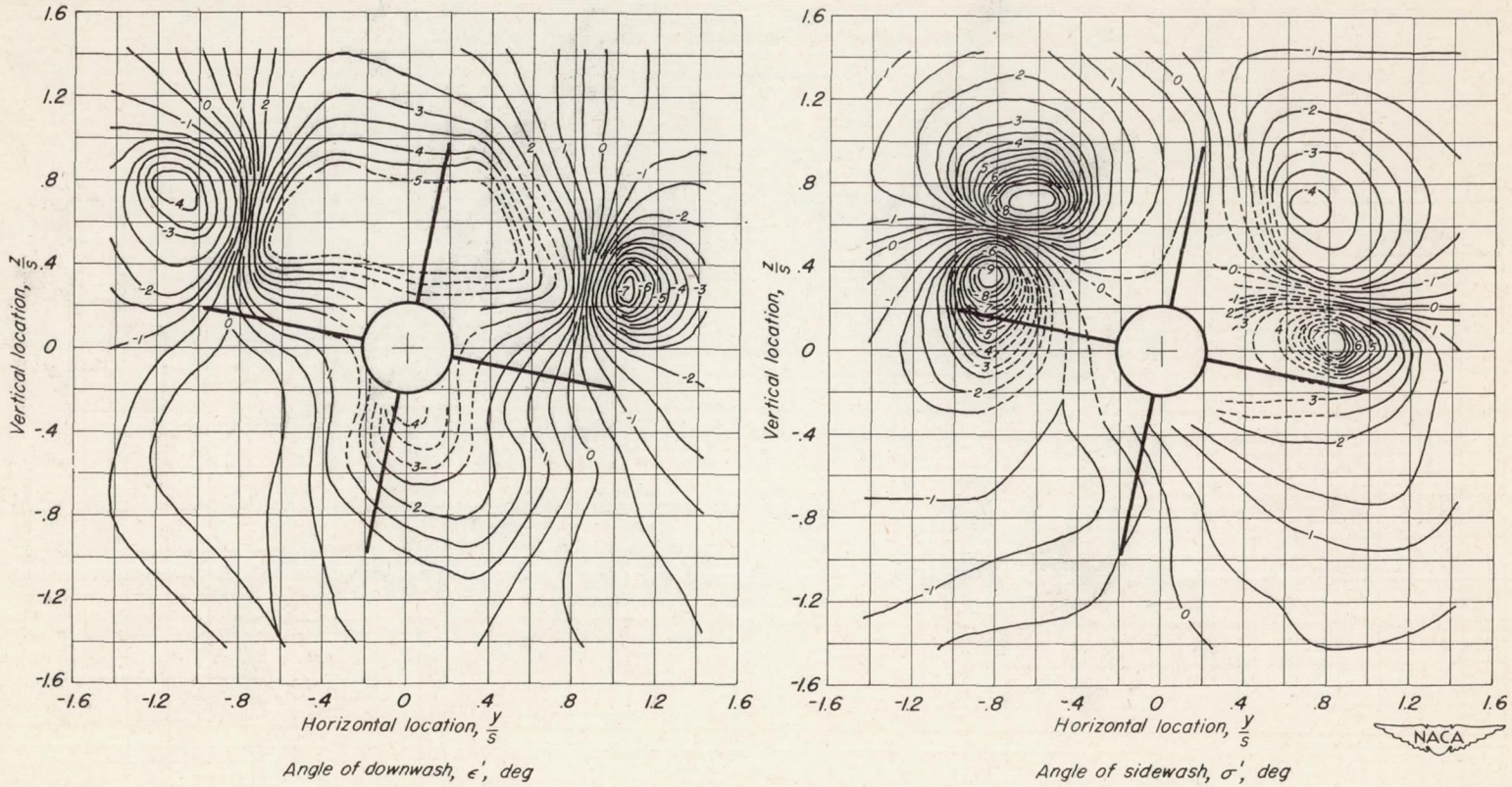

(d) $\alpha = 8°$

Figure 4.–Concluded.

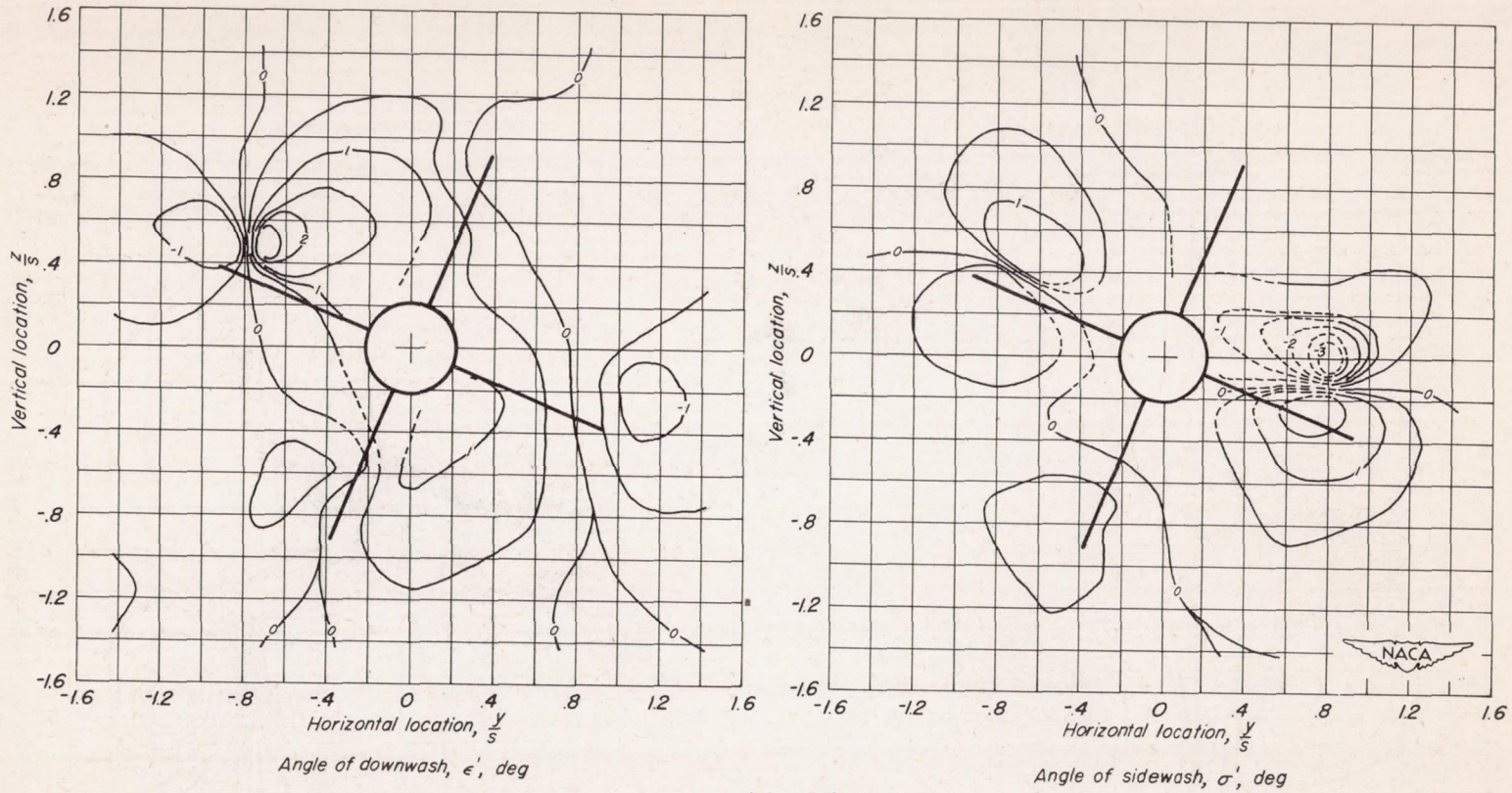

(a) $\alpha = 2°$

Figure 5.—Contours of constant angles of downwash and sidewash. $\phi = 22\text{-}1/2°$.

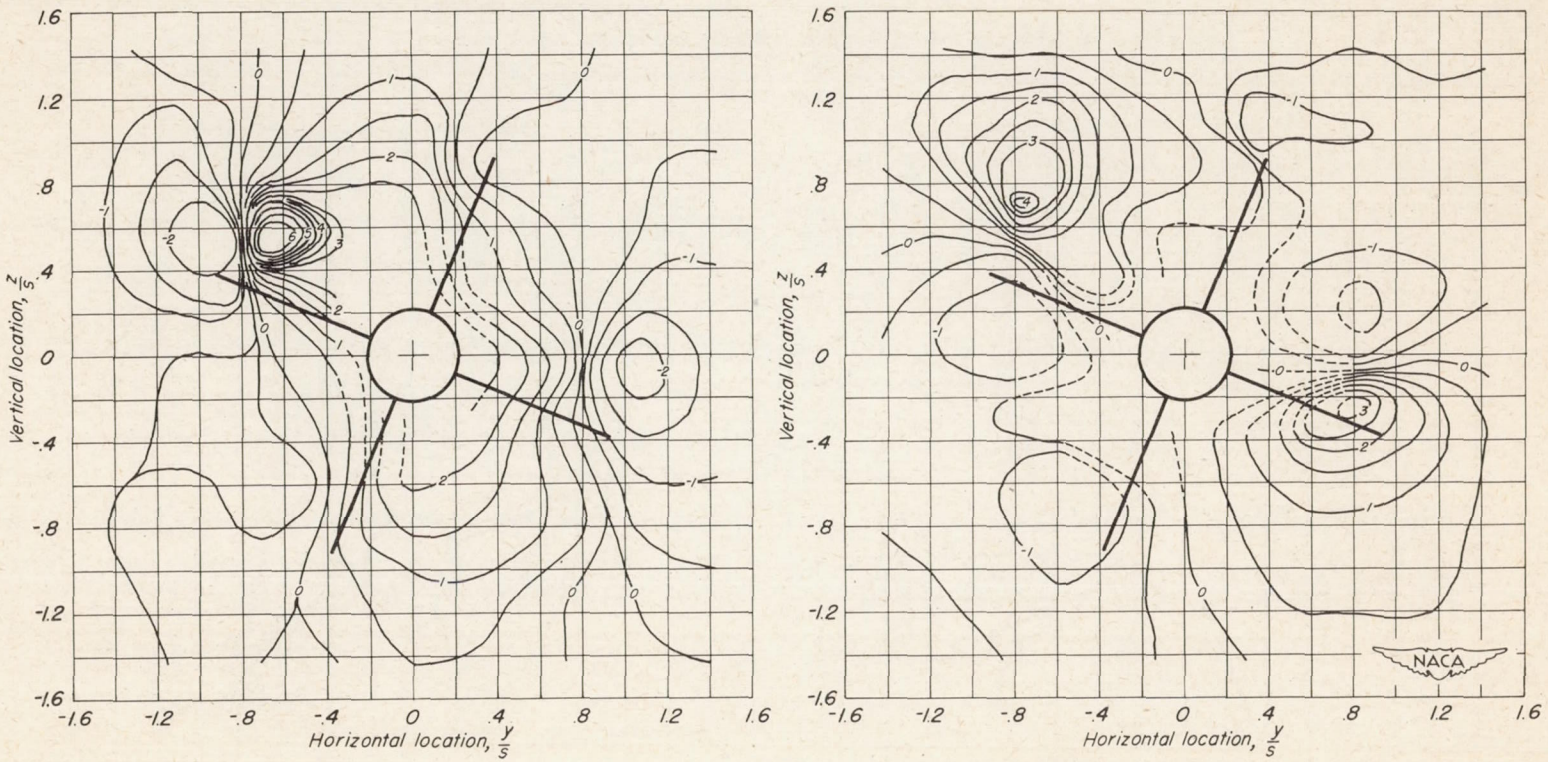

(b) $\alpha = 4°$

Figure 5.—Continued.

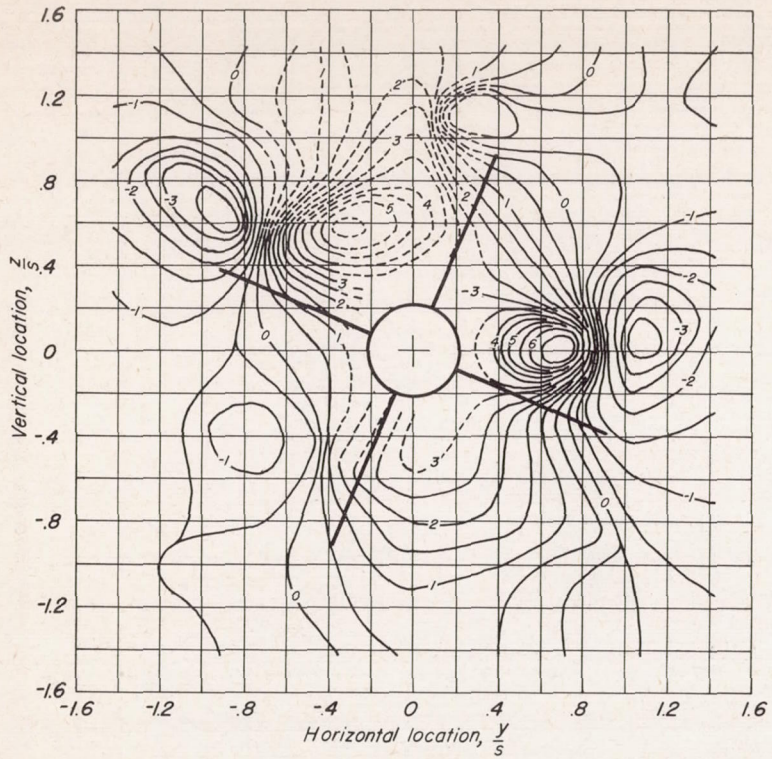

Angle of downwash, ϵ', deg

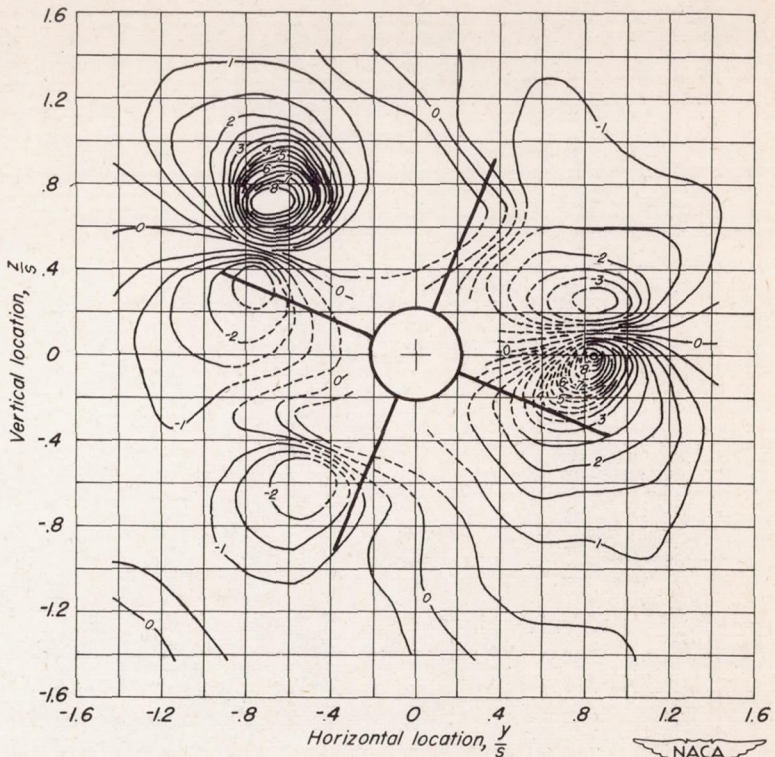

Angle of sidewash, σ', deg

(c) $\alpha = 6°$

Figure 5.—Continued.

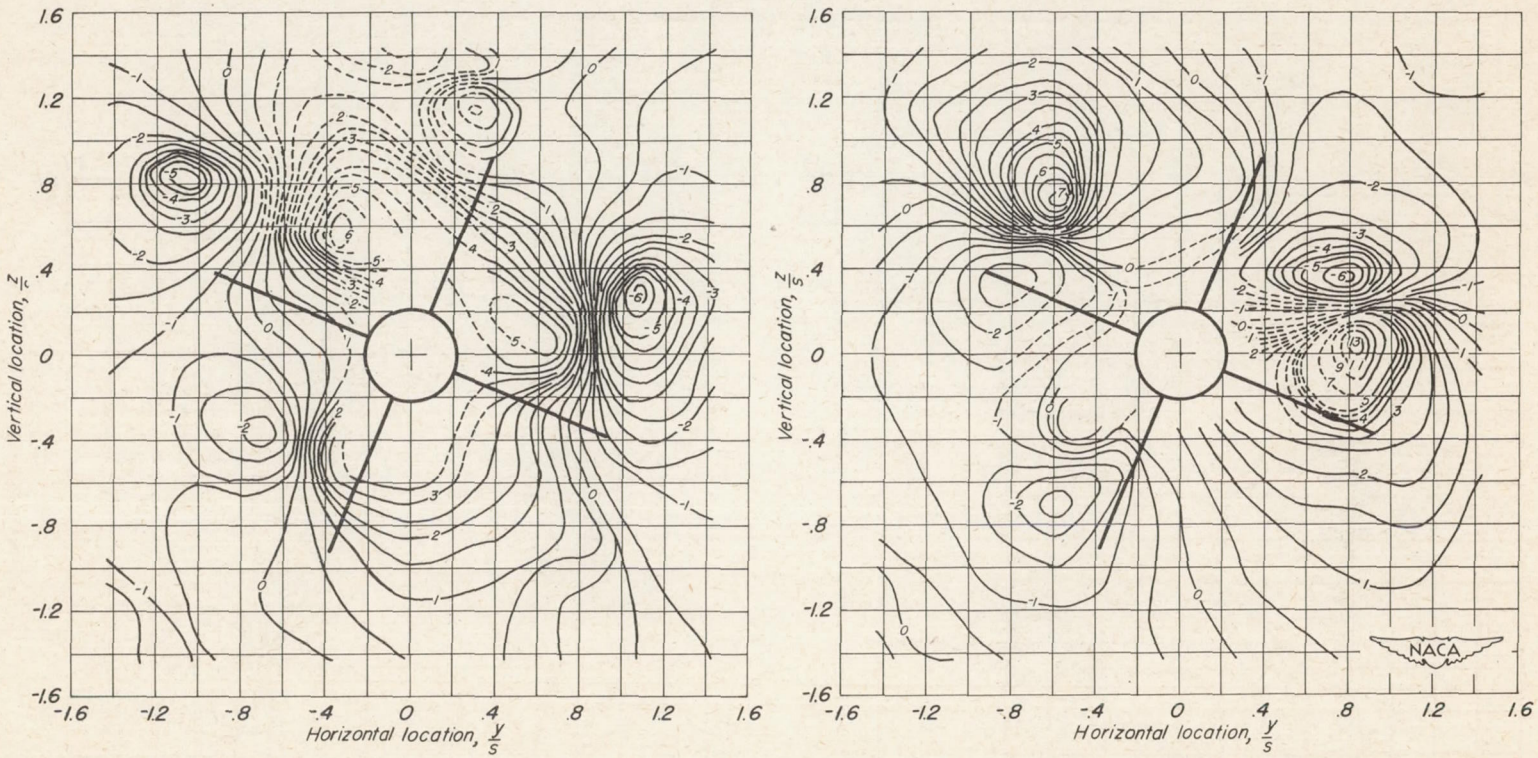

(d) $\alpha = 8°$

Figure 5.– Concluded.

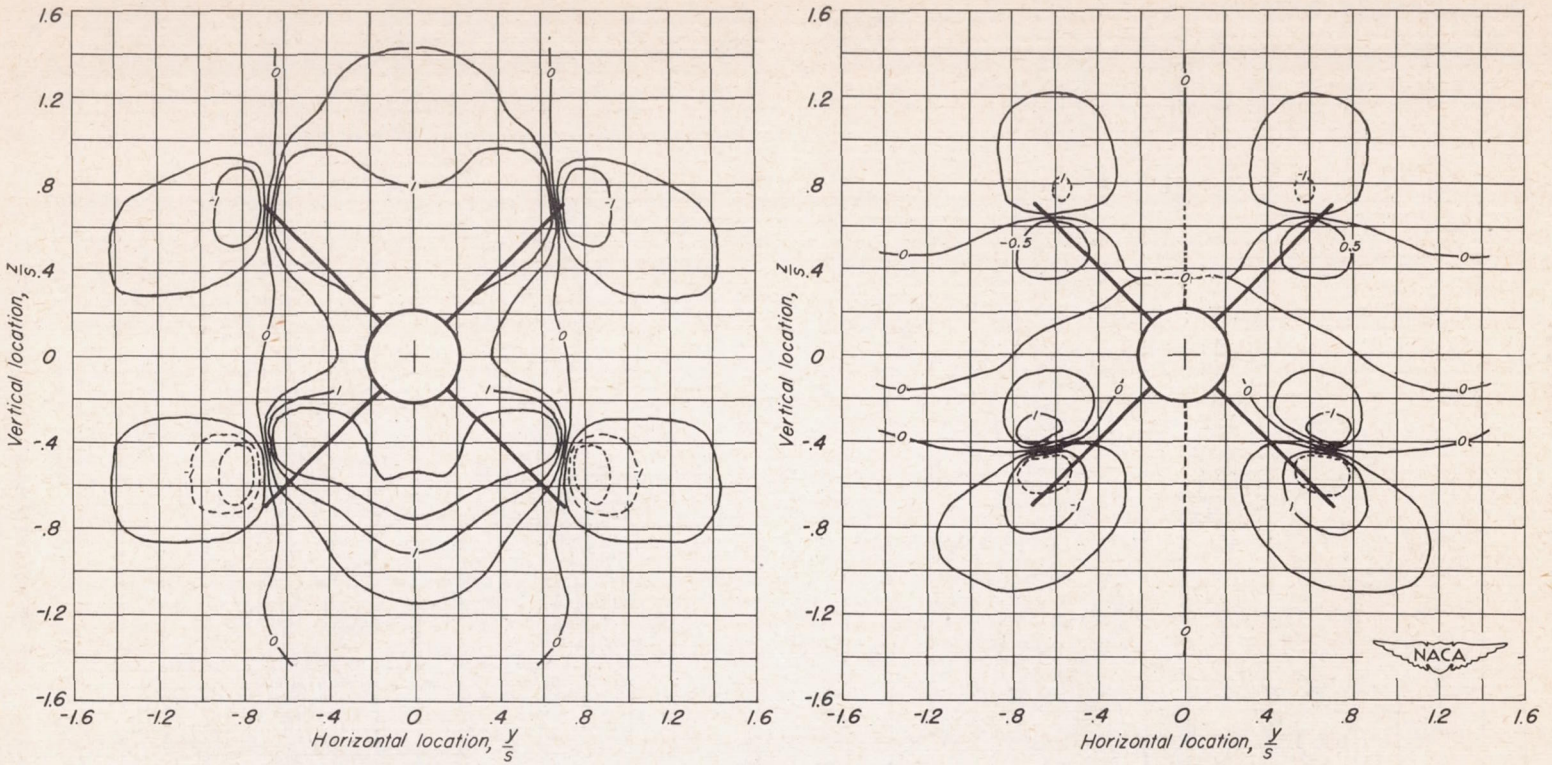

(a) $\alpha = 2°$

Figure 6.—Contours of constant angles of downwash and sidewash. $\phi = 45°$.

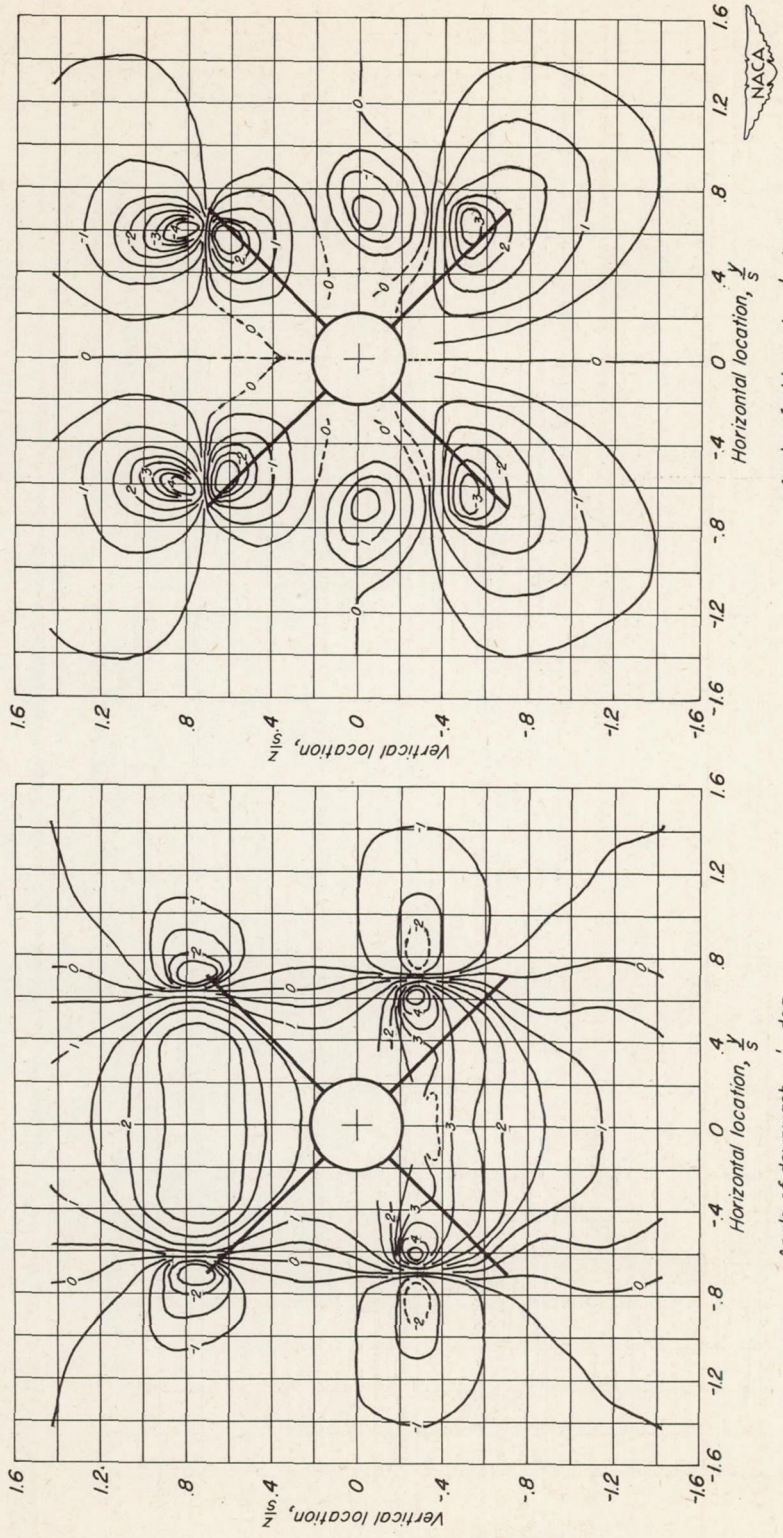

(b) $\alpha = 4°$

Figure 6.—Continued.

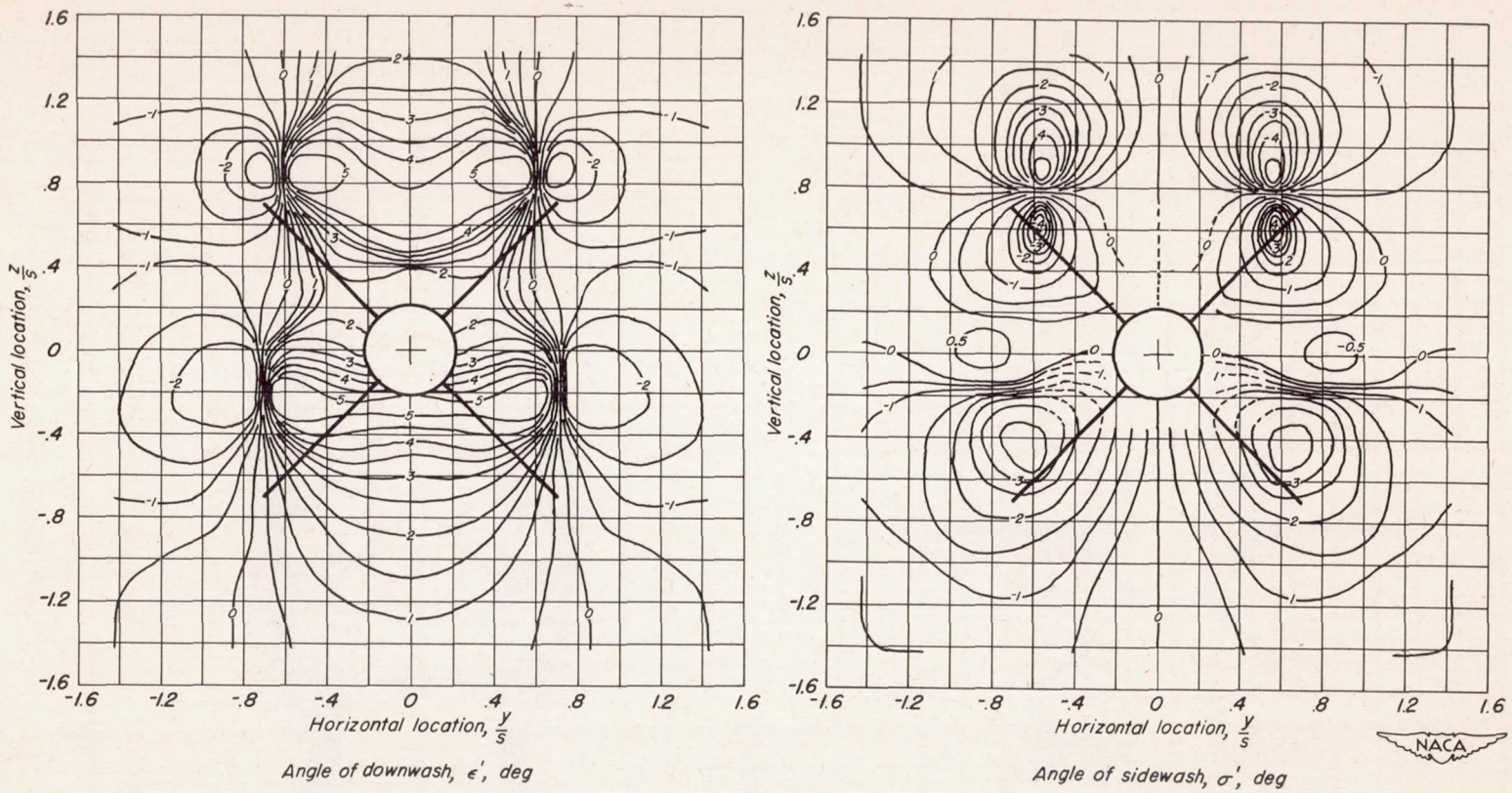

(c) $\alpha = 6°$

Figure 6.—Continued.

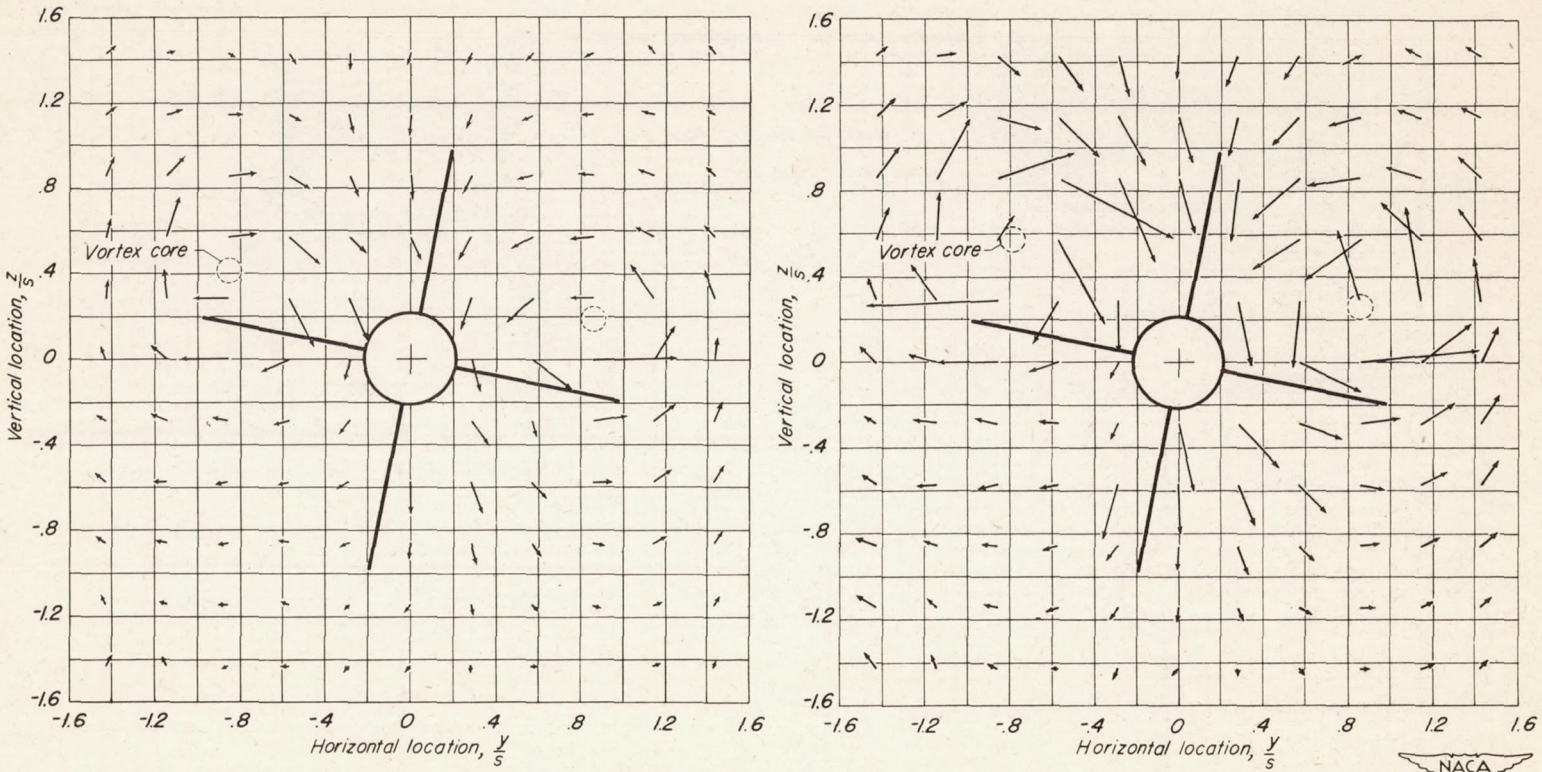

Figure 8.—Vector representation of flow velocities. ϕ=11-1/4°.

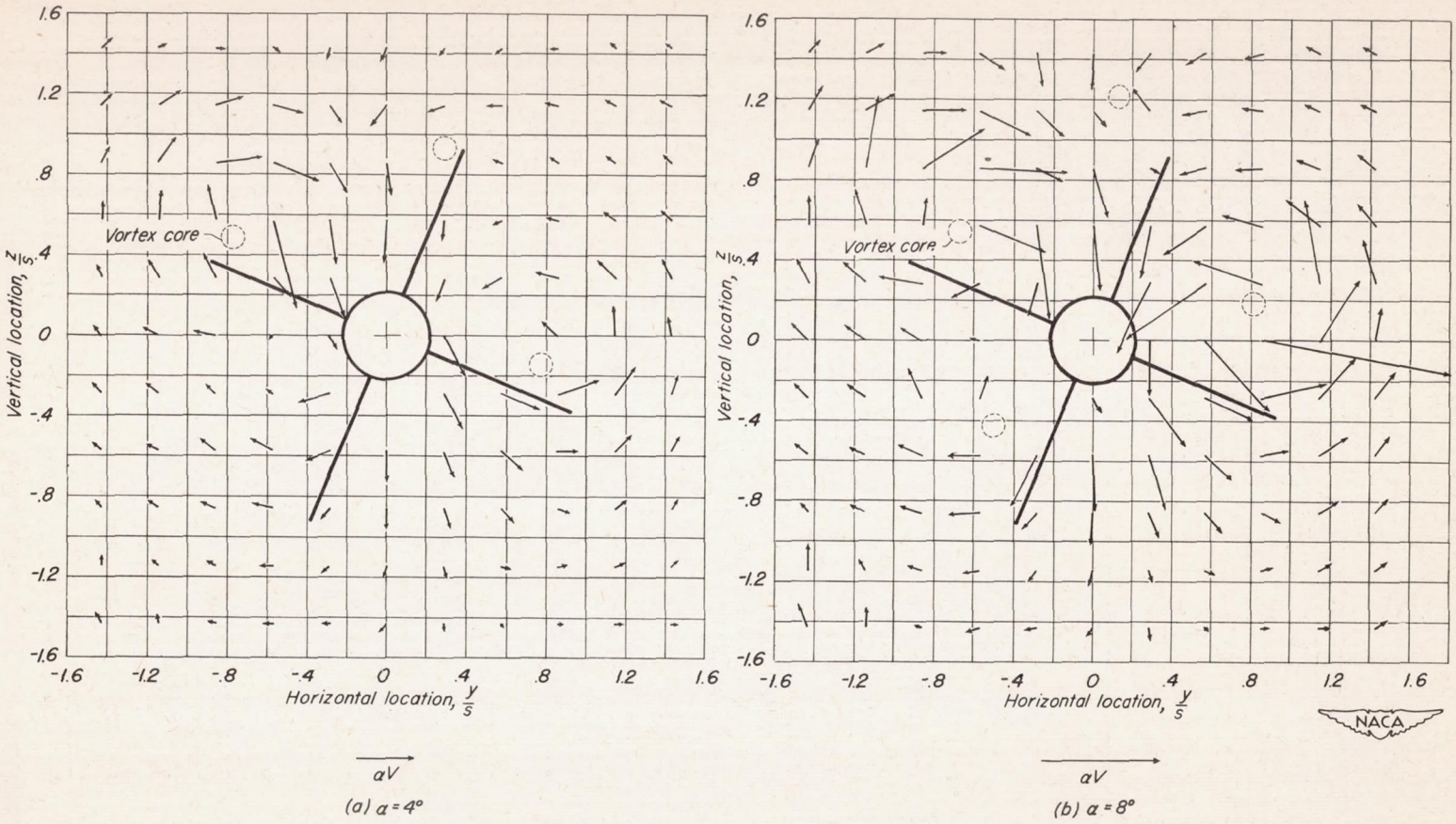

Figure 9.—Vector representation of flow velocities. $\phi = 22\text{-}1/2°$.

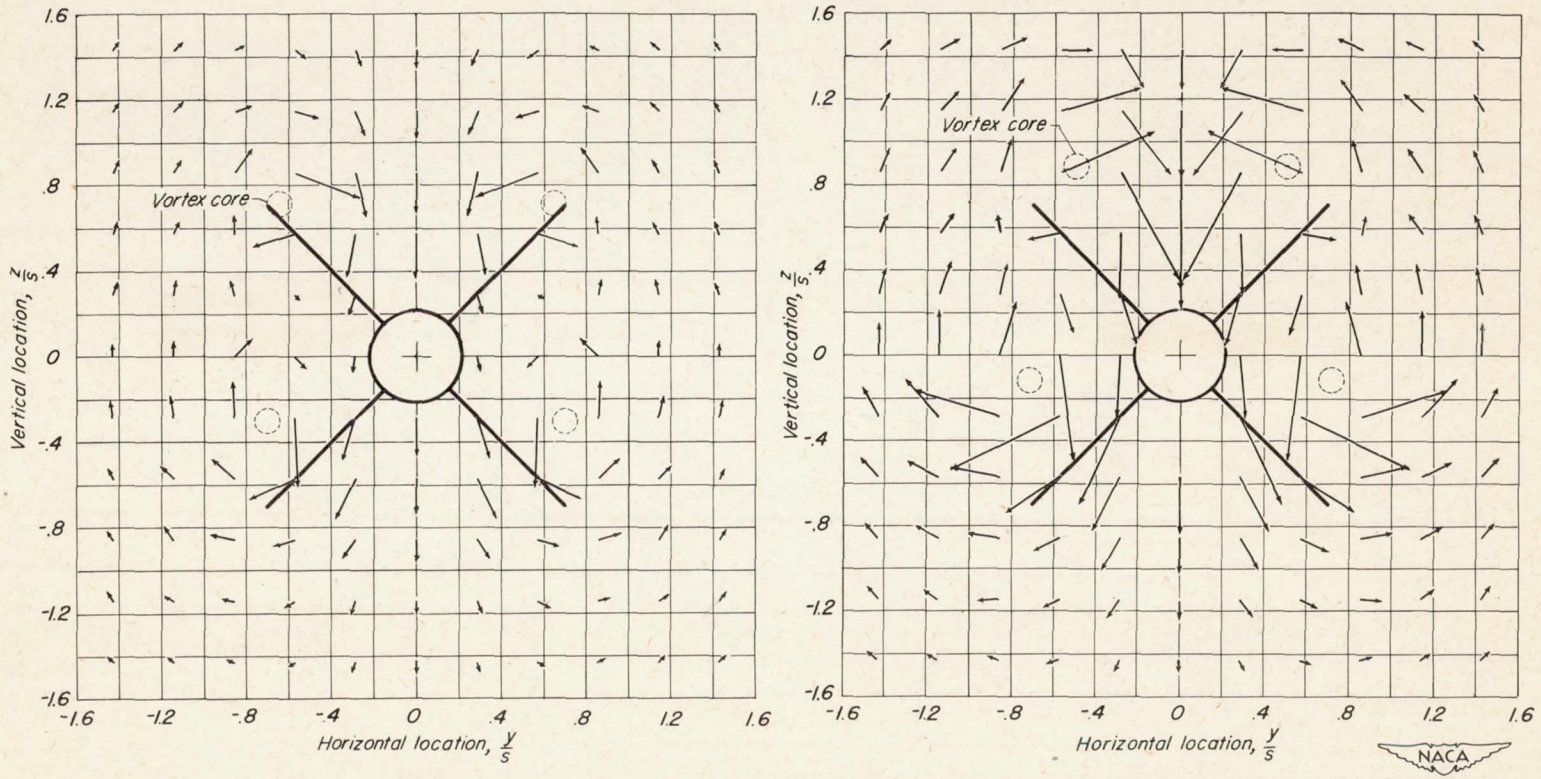

αV

(a) $\alpha = 4°$

αV

(b) $\alpha = 8°$

Figure 10.—Vector representation of flow velocities. $\phi = 45°$.

NACA-Langley - 4-4-51 - 325